

Chapter 4

Growth Mechanism Analysis

The growth mechanism of Spray ILGAR CuInS₂ thin films is analyzed in this chapter, in order to deduce a growth model. In particular, such a growth model should explain the bilayered morphology of the deposited films that was observed in chapter 3 (Fig. 3.13d).

As described in chapter 3, the Spray ILGAR CuInS₂ thin films are prepared in a cyclic process (*Spray ILGAR process*), in which a precursor layer is deposited by spraying on a substrate (*spray step*) and subsequently sulfurized by H₂S (*H₂S step*) in each cycle (*ILGAR-cycle*). In order to remove secondary phases (In₂O₃ and Cu_{2-x}S; section 3.3.2.) from these *as-deposited* Spray ILGAR CuInS₂ thin films, they have to be annealed in Ar/H₂S and etched in KCN after deposition. In each of these process steps (spray step, H₂S step, post-deposition H₂S annealing, KCN etching), chemical reactions between the phases, which are present in the film at the specific stage of the process, occur. In order to enable the deduction of a growth model, these phases have to be identified. This was done by analyzing the composition and the distribution of the different phases in the deposited thin films after each of these process steps separately.

As a basis for the following sections, section 4.1. briefly summarizes the physical principles, which govern chemical reactions and phase transformations in solids.

In section 4.2., the composition of the precursor layers, which are deposited in the spray step of the ILGAR-cycle, is investigated by elastic recoil detection analysis (ERDA), X-ray diffraction (XRD), X-ray fluorescence spectroscopy (XRF) and X-ray Auger spectroscopy (XAS). Based on the results of these investigations, possible mechanisms for the processes during the spray step are discussed.

The sulfurization of the deposited precursor layers, which occurs during the H₂S step of the ILGAR-cycle, is discussed in section 4.3.

The composition of the as-deposited Spray ILGAR CuInS₂ thin films (i.e. after completion of the Spray ILGAR process) is subsequently analyzed. Additionally, the compositional changes that are caused by the post-deposition H₂S and KCN treatments are studied by XRF and XRD in section 4.4.1. In section 4.4.2., the local distribution of the different elements and phases in the films (CuInS₂, Cu_{2-x}S, In₂O₃, carbon) is investigated on the basis of the results of section 4.4.1. Therefore, morphological characterization (SEM and transmission electron microscopy (TEM)) was combined with spatially resolved (energy-filtered TEM, energy-dispersive X-ray spectroscopy (EDX)) and surface-sensitive (X-ray photoelectron spectroscopy (XPS) and Auger spectroscopy (XAS)) analysis of the chemical composition of the thin films.

From the spatial distribution of the elements in the films, which is revealed in section 4.4., conclusions about the diffusion paths of these elements during the growth process can be drawn. A model for the growth of Spray ILGAR CuInS₂ thin films is proposed in section 4.5., which is based on these deductions. In section 4.6., future modifications of the Spray ILGAR process for CuInS₂ thin films are discussed on the basis of the proposed growth model.

All samples, which are discussed in this chapter, were deposited onto molybdenum-coated glass substrates using the setup shown in Fig. 3.3. If not stated otherwise, the preparation parameters were identical to those in Table 3.6. An overview of all preparation parameters of the samples is given in Appendix I.

The analysis techniques which have been applied for the measurements of this chapter are described in Appendix VII.

4.1. Chemical Reactions and Phase Transformations in Solids

In this section, the physical principles which determine the occurrence of a chemical reaction or a phase transformation in a solid are briefly discussed. Firstly, the energetic aspects of such processes are discussed. Afterwards, the kinetics of such processes is considered. The third part of this section focuses on phase transformations and reactions in which diffusion is the dominating mechanism. For a more detailed discussion of these processes, the reader is referred to Ref. [Haasen '91].

Solids constitute ensembles of atoms or molecules. As do all physical systems, solids seek to reach a state of minimal free energy G . The free energy of a system is defined as:

$$G \equiv H - TS = U + pV' - TS, \quad \text{Eq. (4.1)}$$

where H is the free enthalpy, S is the entropy, T is the temperature, U is the internal energy, p is the pressure and V' is the volume of the system [Kubaschewski '93]. For the case of constant temperature and pressure, the change of the free energy ΔG of a given system in thermal equilibrium is then given by the changes the free enthalpy ΔH and the entropy ΔS :

$$\Delta G = \Delta H - T \cdot \Delta S, \quad \text{Eq. (4.2)}$$

In order to assess, if a chemical reaction or phase transformation is thermodynamically favorable, ΔG can be calculated from Eq. (4.2.) using tabulated values for the standard free enthalpies and entropies of the products and educts of the respective reaction or phase transformation. In Appendix X, values for the standard free enthalpies and entropies are listed for various compounds, which are relevant for the processes analyzed in this chapter.

For a system which contains different amounts n_i of N different species i , the total differential of the free energy can be expressed by the Gibbs-Duhem-equation:

$$dG = -SdT + V'dp + \sum_{i=1}^N \mu_i dn_i \quad \text{Eq. (4.3)}$$

In Eq. (4.3), μ_i is the chemical potential of the species i . All processes which are discussed in this thesis take place at ambient pressure. Therefore, $dp = 0$ mbar is valid in all cases. Thus, for a given system, either a change of temperature or of the amount of species i (i.e. its concentration) lead to a change of the free energy. This means that a system will react to a change in temperature by converting one species i into another j , in order to minimize its free energy, i.e. by a chemical reaction or phase transformation. If the temperature is also constant, a change in concentration of one species may also initiate a chemical reaction or phase transformation.

Kinetics of Temperature-Activated Processes

From Eq. (4.1-3), no information is given about the time scale on which a process proceeds. These kinetic aspects are discussed in the following for the case of isothermal processes. Since no temperature gradients were applied during the various process steps, all processes investigated in this thesis can be regarded as isothermal.

The variables ζ of a process (e.g. the quantity of a species, layer thickness, etc.) can be described by the fractional conversion $f_c = \zeta/\zeta_{\max}$ of the respective variable. The time-dependence of f_c can be expressed by Eq. (4.4) [Sestak '73], [Koch '83]:

$$\frac{df_c}{dt} = k(T) \cdot f_c^m (1 - f_c)^n (-\ln(1 - f_c))^p, \quad \text{Eq. (4.4)}$$

where $k(T)$ is the rate of the process. The constants m , n and p depend on the dominating reaction mechanism. The values for m , n and p for different kinds of process mechanisms are listed and discussed in Ref. [Koch '83].

The reaction rate $k(T)$ of a temperature-activated process follows the Arrhenius equation:

$$k(T) = k_\infty \cdot \exp\left(-\frac{E_A}{k_B T}\right) \quad \text{Eq. (4.5)}$$

Here, k_∞ is the frequency factor, which formally corresponds to the reaction rate at infinite temperature. E_A is the activation energy of the process and k_B is the Boltzmann-constant.

A special kind of temperature-activated processes are diffusion-limited reactions. This means that the rate of these processes is limited by the transport of the educts and products to and away from the reaction site, respectively. Reactions in which one of the reaction partners is a solid are frequently observed to be diffusion-limited. In the following, diffusion processes in solids are discussed.

Diffusion-Controlled Reactions in Solids

If a concentration gradient of a species exists in a system, the gradient prevents the thermal equilibrium of the system. Therefore, the system seeks to level the gradient by the diffusion of particles in order to reach equilibrium. The dependence of the current density of the diffusing particles j_D on the gradient of the concentration c of the diffusing species is described by Fick's first law:

$$\mathbf{j}_D = -D_{A_x B_y}^A \cdot \nabla c \quad \text{Eq. (4.6)}$$

Here, $D_{A_x B_y}^A$ is the diffusion coefficient of the diffusing species A in the compound $A_x B_y$. $D_{A_x B_y}^A$ is a function of the temperature. This can be understood if one takes into account that an atom in a solid has to leave its site in the crystal lattice, before it can diffuse through the solid. Thus, its lattice bonds must be broken, which means that its diffusion is hindered by an energy barrier. The probability that the energy of an atom is sufficiently high to pass this barrier is determined by the statistics of Boltzmann and therefore increases with temperature. The temperature dependence of $D_{A_x B_y}^A$ is expressed in Eq. (4.7):

$$D_{A_x B_y}^A(T) = D_0 \cdot \exp\left(-\frac{E_A}{k_B T}\right) \quad \text{Eq. (4.7)}$$

Here, E_A is the activation energy and D_0 is a material constant. In analogy to Eq. (4.5), D_0 is called the frequency factor. The values for $D_{A_x B_y}^A$, D_0 and E_A , which were used in the course of this thesis, are compiled in Appendix V.

The kinetics of reactions in which at least one reaction partner is a solid can be described by the reactive diffusion model. This model was discussed by Dybkov [Dybkov '86; Dybkov_1 '86; Dybkov_2 '86]. In the following, the main results of this discussion are considered.

If two substances A and B are brought into contact with each other, there will be a jump in the concentration profile across their interface at the beginning of the process ($t=0$ s). For the sake of simplicity, it is assumed in the following that A and B are elemental substances, which

solely consist of atoms of element A and B, respectively. Then, if both elements can react with each other, a thin layer of the compound $A_\alpha B_\beta$ will be formed at the interface in the following ($t > 0$ s). Depending on the composition range of $A_\alpha B_\beta$, the atoms A and B can diffuse through this layer in order to level the concentration gradient. Thus, the formation reaction of $A_\alpha B_\beta$ can proceed at both sides of the interface layer. Thereby, the thickness x of the interface layer will increase and the concentrations of A and B are assumed to evolve linearly within this layer, but still to exhibit jumps at the interfaces A/ $A_\alpha B_\beta$ and $A_\alpha B_\beta$ /B. In the following, $D_{A_\alpha B_\beta}^A \gg D_{A_\alpha B_\beta}^B$ is assumed, i.e. A diffuses much faster than B in $A_\alpha B_\beta$. For very thin layers of $A_\alpha B_\beta$, all atoms of A can diffuse quickly through the interface layer and react to further $A_\alpha B_\beta$ at the interface A/ $A_\alpha B_\beta$. Therefore, the rate of the process will only depend on the reaction rate k_R of the net chemical reaction $\alpha A + \beta B \rightarrow A_\alpha B_\beta$ and x will increase linearly in time:

$$x = k_R \cdot t \quad \text{Eq. (4.8)}$$

As soon as the thickness x has increased to such an extent that the formation of $A_\alpha B_\beta$ proceeds faster than the diffusion of A through the $A_\alpha B_\beta$ layer, the reaction is diffusion-limited. In this case the formation process of $A_\alpha B_\beta$ has to proceed at a rate $k < k_R$ due to the lack of A at the interface B/ $A_\alpha B_\beta$. For diffusion-limited reactions the thickness increases parabolically:

$$x = \sqrt{2k_D \cdot t} \quad \text{Eq. (4.9)}$$

Here, k_D is the diffusion-limited reaction rate. It is determined by the diffusion coefficient of the fastest diffusing species (A) and the concentration gradient between the interfaces A/ $A_\alpha B_\beta$ and $A_\alpha B_\beta$ /B:

$$k_D = \frac{D_{A_\alpha B_\beta}^A \cdot (c_{A;B/A_\alpha B_\beta} - c_{A;A/A_\alpha B_\beta})}{c_{A;A/A_\alpha B_\beta}} \quad \text{Eq. (4.10)}$$

Here, $c_{A;X/A_\alpha B_\beta}$ is the concentration of A at the interface X/ $A_\alpha B_\beta$, where X is either A or B. For long process durations, the layer thickness x of the $A_\alpha B_\beta$ layer approaches the diffusion length L_D of the diffusing species in the diffusion-limited case:

$$x \approx \sqrt{D \cdot t} = L_D \quad \text{Eq. (4.11)}$$

Additional Influences on the Diffusion in Solids

In the following, it is qualitatively described how the diffusion properties of solids, as described by the above equations, are altered by the presence of electric fields and structural defects, such as vacancies or grain boundaries, in the solid. However, since these influences will only be discussed qualitatively in the following sections, they are also not described quantitatively in this section.

So far, the diffusion processes have been described as they occur in metals, in which, electrons can move freely and thus can be regarded as an electron gas. Therefore, the diffusing ions can be treated as neutral particles.

In contrast, the charge of the diffusing ions has to be taken into account for materials which contain ionic bonds. In thin layers, especially at low temperatures, electric fields, which may build up at interfaces, can influence the diffusion. In this case, the diffusion of the ions in the crystal is determined by their electrochemical potential $\eta_i = \mu_i + z_i \cdot F \cdot \varphi$, instead of their chemical potential μ_i (Eq. (4.3.)). Here, z_i is the charge of the diffusing species, F is the Faraday constant ($F = 96500$ As) and φ is the electric potential.

In particular, surface reactions in oxidation or sulfurization processes of semiconductors can induce surface fields. These fields can result in either the accumulation or the depletion of a

certain species in the surface-near region of the layer. Depending on the rate of the surface reactions, linear, parabolic, logarithmic, as well as cubic growth rates have been observed for the surface layer thickness x . A detailed description of alterations of the diffusion behavior induced by electric fields is given in Ref. [Ritchie '69; Ritchie_1 '69].

Furthermore, the diffusion behavior in solids is influenced by the presence of structural defects, such as vacancies or grain boundaries. The vacancies as well as the grain boundaries constitute additional diffusion paths for the diffusing species. These additional paths have been neglected in the previous discussion. Therefore, the diffusion in polycrystalline materials like the CuInS_2 thin films, which are investigated in this thesis, can be expected to proceed faster than predicted by Eq. (4.6-11). Generally, the activation energy for grain boundary diffusion is lower than for bulk diffusion. Hence the former is the dominating diffusion mechanism at low temperatures, whereas the bulk diffusion dominates at high temperatures.

For a detailed discussion of the influence of grain boundaries and vacancies of the diffusion in solids, the reader is referred to Ref. [Haasen '91; Kaur '95].

4.2. Precursor Layer Deposition

The Spray ILGAR CuInS_2 thin films are deposited from mixed acetone-based spraying solutions of $\text{Cu}(\text{hfac})_2$ and InCl_3 (section 3.3.2.). As a first step in the deduction of a growth model for Spray ILGAR CuInS_2 thin films, this section focuses on the identification of the copper- and indium-containing precursor compounds, which are deposited during the spray step of the ILGAR-cycle, i.e. prior to sulfurization, as well as on the mechanisms that govern their deposition.

In order to understand the mechanisms of thin film deposition from mixed acetone solutions of $\text{Cu}(\text{hfac})_2$ and InCl_3 , it is important to consider possible interactions between the two compounds that may influence the deposition process. This section starts with separate discussions of the deposition processes from pure $\text{Cu}(\text{hfac})_2/\text{acetone}$ (section 4.2.1.) and from pure $\text{InCl}_3/\text{acetone}$ solutions (section 4.2.2.). The interactions that are observed in the deposition process from mixed solutions of $\text{Cu}(\text{hfac})_2$ and InCl_3 are subsequently studied in section 4.2.3.

The thickness of a precursor layer, which is deposited in a single spray step under conditions as they are used for the deposition of Spray ILGAR CuInS_2 thin films (Table 3.6), is in the range of 10-30 nm (section 3.1.3.). Due to the small amount of material (about 10^{16} atoms/cm²), such a thin layer cannot be characterized precisely by bulk-sensitive analysis techniques like XRD or XRF. On the other hand, the results of surface-sensitive measurements like XPS or XAS may be influenced by adsorbed species at the layer surface. Therefore, in this section, thin films are discussed, which were prepared by repeating 10-20 spray steps without any H_2S step in order to obtain thicknesses in the range of several hundred nanometers, which allow for the use of XRF and XRD⁵.

4.2.1. Deposition of a Copper-Containing Precursor Compound

For the Spray ILGAR deposition of CuInS_2 thin films, a mixed acetone solution of $\text{Cu}(\text{hfac})_2$ and InCl_3 is used as a spraying solution (section 3.3.2.). This section focuses on the identification of the copper-containing precursor compound that is deposited in the spray step of the process. In order to understand the deposition mechanism of this compound only pure $\text{Cu}(\text{hfac})_2/\text{acetone}$ solutions, *in the absence of InCl_3* , are investigated in this section. To what

⁵ In principle, such films could be deposited by continuous spraying for an extended duration. However, in order to avoid cooling of the substrate due to the evaporation of acetone (section 2.3.; p. 20) and to mimic the thermal conditions of the Spray ILGAR process, the spraying was interrupted by breaks of 10 sec.

extent the presence of InCl_3 alters this deposition process will be discussed in section 4.2.3.

Identification of the Copper-Containing Precursor Compound

A Spray ILGAR deposited thin film was grown (sample 401) by spraying 12.5 ml of a 40 mM $\text{Cu}(\text{hfac})_2/\text{acetone}$ solution in repeated spray steps of 20 s (12 spray steps) without sulfurization. To allow comparison, these values are in the same range as those used for the deposition of Spray ILGAR CuInS_2 thin films (Appendix I). The as-grown film was investigated by grazing incidence XRD (0.5°) in order to identify the copper-containing compound.

Fig. 4.1 shows the X-ray diffractogram that was obtained from this thin film. It is dominated by reflections of copper (JCPDS 00-004-0836) and molybdenum (JCPDS 00-042-1120), the latter stemming from the substrate. Additionally, reflections of MoO_2 (JCPDS 01-078-1069) and of $\text{MoO}(\text{OH})_2$ (JCPDS 00-009-0161) were observed. This indicates that the molybdenum surface was partially oxidized during the spray process. This is likely due to the reaction of molybdenum with H_2O , which comes from the hydrated $\text{Cu}(\text{hfac})_2$ compound (Fig. 3.1.).

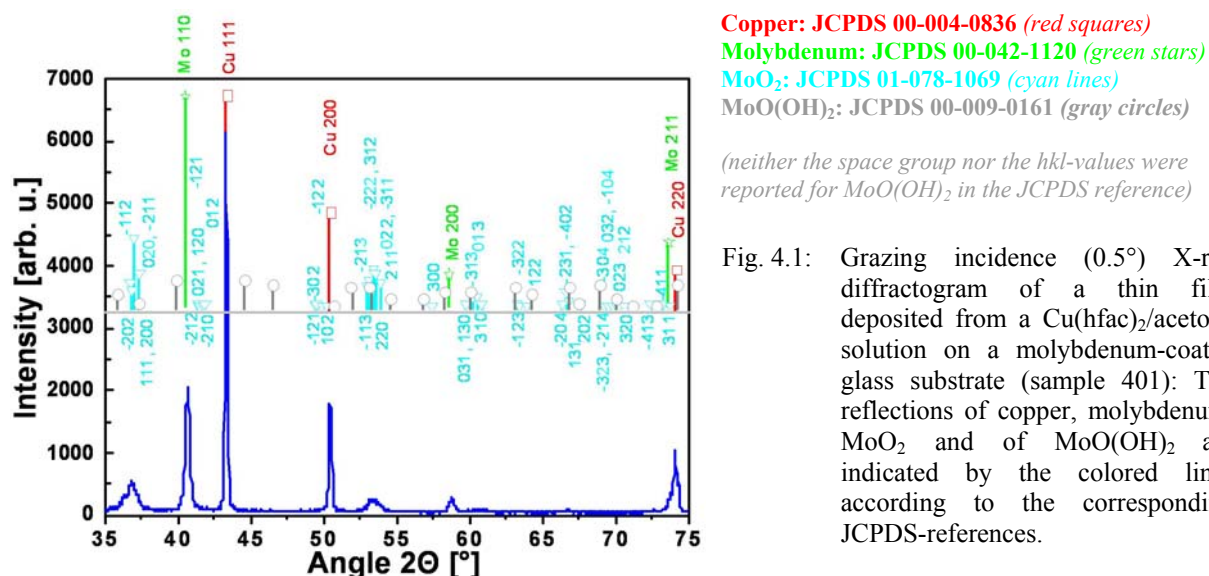


Fig. 4.1: Grazing incidence (0.5°) X-ray diffractogram of a thin film deposited from a $\text{Cu}(\text{hfac})_2/\text{acetone}$ solution on a molybdenum-coated glass substrate (sample 401): The reflections of copper, molybdenum, MoO_2 and of $\text{MoO}(\text{OH})_2$ are indicated by the colored lines according to the corresponding JCPDS-references.

This result shows that under the conditions which are used for the deposition of Spray ILGAR CuInS_2 thin films, the spraying of $\text{Cu}(\text{hfac})_2/\text{acetone}$ solutions leads to the deposition of metallic copper. This agrees with reports about the deposition of copper films by atomic layer deposition (ALD) using $\text{Cu}(\text{hfac})_2$ as a precursor [Törndahl '04], since the deposition mechanism of ALD is similar to that of the Spray ILGAR process (section 2.3.).

Mechanism of Copper Deposition by Spraying of $\text{Cu}(\text{hfac})_2/\text{Acetone}$ Solutions

For the sake of clarity, it is important to differentiate between the compounds copper(II)hexafluoroacetylacetonate hydrate ($\text{Cu}(\text{hfac})_2$), the unhydrated copper(II)hexafluoroacetylacetonate ($\text{Cu}^{\text{II}}(\text{hfac})_2$) and copper(I)hexafluoroacetylacetonate ($\text{Cu}^{\text{I}}(\text{hfac})$). In Fig. 4.2a-e, the molecular structures of these compounds are depicted together with those of hexafluoroacetylacetonate (H-hfac) and of a radical formed from the hfac group ($\cdot\text{hfac}$).

Even though numerous publications about the deposition of copper thin films using $\text{Cu}(\text{hfac})_2$ as a precursor compound in chemical vapor deposition (CVD) or ALD processes exist [Cohen '92; Lecohier '92; Kim '98; Törndahl '04], the reaction mechanism is still not understood completely. It is known that either H_2 or H_2O are needed in order to avoid carbon contamination during the deposition process [Temple '89; Cohen '92; Lecohier '92].

Generally, these reactants are needed to remove adsorbed carbon-containing hfac groups from the substrate surface. H₂ or H₂O can either be provided directly as additional reactants or by using the hydrated compound Cu(hfac)₂. Hydrated Cu(hfac)₂ was used in the Spray ILGAR deposition process presented here. The role of H₂O in absence of H₂ is, however, controversially discussed [Cohen '92; Lecohier '92; Kim '98].

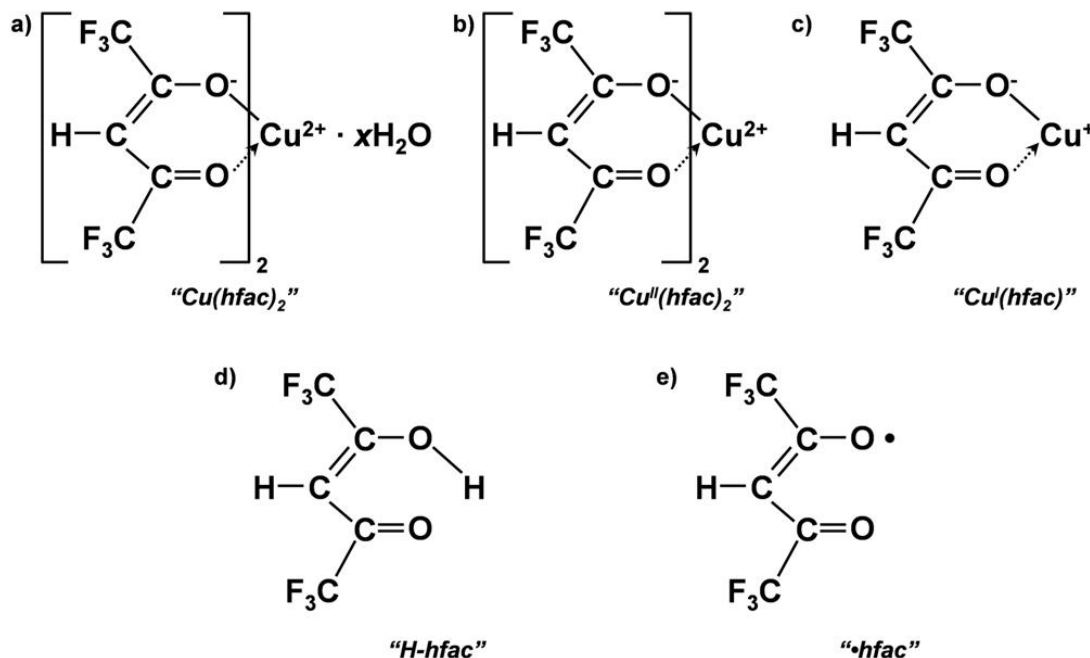
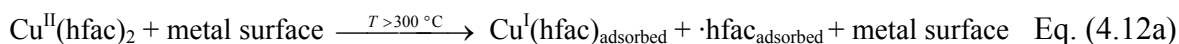


Fig. 4.2: Molecular structures and abbreviations for the different species involved in the deposition process of copper in the spray step of the ILGAR-cycle. The bond lengths and angles are not drawn to scale. a) Copper(II)hexafluoroacetylacetonate hydrate [Sigma_2 '08]; b) unhydrated copper(II)hexafluoroacetylacetonate [Sigma_2 '08]; c) monovalent copper(I)hexafluoroacetylacetonate [Hampden-Smith '95]; d) hexafluoroacetylacetone (enol form) [Nigg '98; Buemi '00]; e) proposed radical formed from the hexafluoroacetylacetonate group.

In the following, a reaction scheme for the deposition of copper by spraying of a Cu(hfac)₂/acetone solution is proposed. The reaction scheme is similar to the models presented in Ref. [Cohen '92] and [Lecohier '92] for the CVD of copper. This model assumes conditions as they are present during the spray step of the Spray ILGAR deposition process of CuInS₂ thin films (Table 3.6). In particular, a metallic substrate (molybdenum or copper) at a temperature of 430 °C and an inert atmosphere (nitrogen) are assumed. The different steps of the proposed deposition process are shown schematically in Fig. 4.3a-f and are discussed in the following.

As the Cu^{II}(hfac)₂ molecules approach the heated substrate, they start to decompose thermally ($T_{\text{decomposition}} \approx 300$ °C [Naik '95]). At the molybdenum surface (Fig. 4.3a), Cu^{II}(hfac)₂ dissociates to an adsorbed Cu^Ihfac species and an adsorbed hfac group, presumably in form of a radical ·hfac [Cohen '92; Lecohier '92].

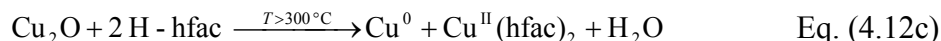


This reaction can readily occur at a metal surface, since free electrons are available and the free electron of ·hfac can directly bond to a surface metal atom. Subsequently, two adsorbed Cu^Ihfac molecules are hydrolyzed to Cu₂O by H₂O releasing two H-hfac molecules [Kim '98] (Fig 4.3b):



In the Spray ILGAR process, H₂O is supplied by using hydrated Cu(hfac)₂. The compound

Cu_2O can then react under disproportionation with further H-hfac (stemming from other reaction sites) to metallic copper, volatile $\text{Cu}^{\text{II}}(\text{hfac})_2$ and H_2O [Kim '98] (Fig. 4.3c):



Alternatively, Cu_2O can decompose directly to copper and O_2 for temperatures above 300°C [Kim '98] (Fig. 4.3d):



At 400°C , the copper film growth is limited by the removal of the blocking $\cdot\text{hfac}$ groups from the substrate surface. This process proceeds via the reaction of H_2O with these groups [Cohen '92; Lecohier '92] (Fig. 4.3e):



Subsequently, the adsorbed OH-groups may leave the surface by reacting with other OH-groups to form H_2O , O_2 and / or H_2O_2 , which desorb subsequently [Lecohier '92] (Fig. 4.3f). After this last step, the reaction sites that were previously blocked by adsorbed hfac groups are free again so that the deposition process will proceed with Eq. (4.12a).

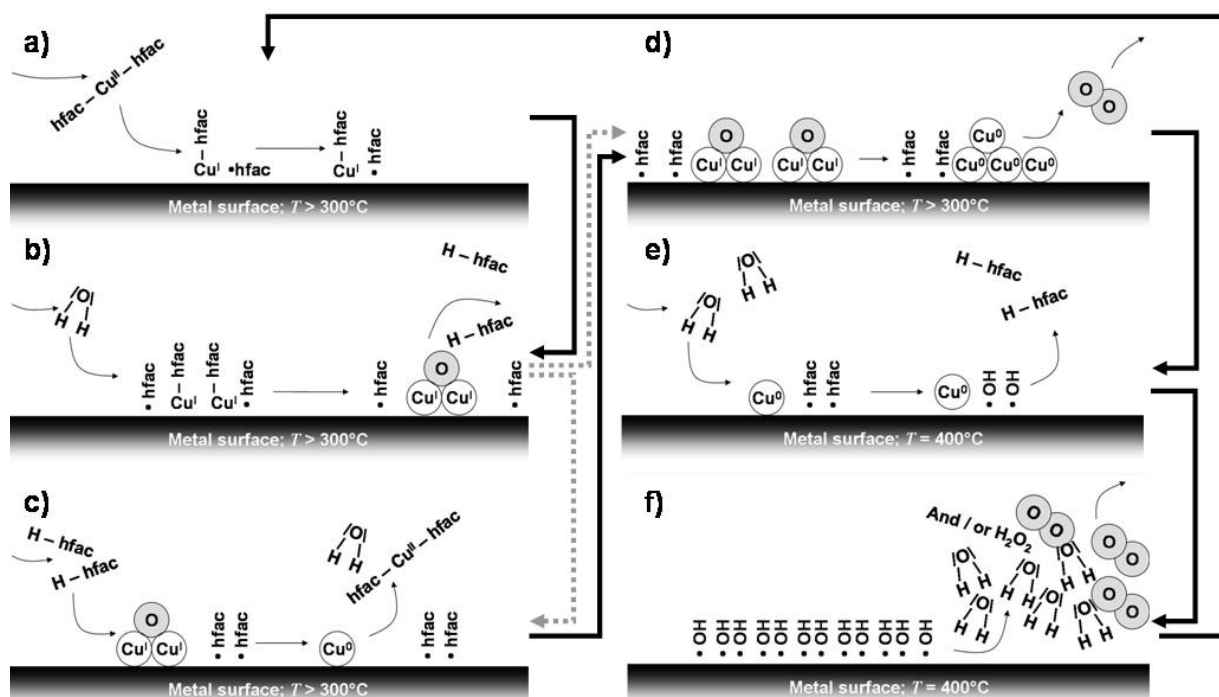


Fig. 4.3: Schematic sketch of the proposed mechanism for the deposition of metallic copper on a metal surface by spraying of a $\text{Cu}(\text{hfac})_2/\text{acetone}$ solution under conditions as in the spray step of the Spray ILGAR deposition process for CuInS_2 thin films: Subfigures a) to f) show the reactions described in Eq. (4.12a) to Eq. (4.12e), respectively. The reaction sequence is indicated by the black arrows; gray arrows indicate alternative processes: a) dissociation of $\text{Cu}(\text{hfac})_2$; b) hydrolyzation of $\text{Cu}^{\text{I}}\text{hfac}$; c) disproportionation of Cu_2O by reacting with H-hfac; d) thermal disproportionation of Cu_2O ; e) removal of $\cdot\text{hfac}$ groups from the surface; f) migration and desorption of adsorbed $\cdot\text{OH}$ groups.

Note that this proposed mechanism (Fig. 4.3a-f) for the deposition of copper can proceed only if H_2O is present. Otherwise the adsorbed hfac groups will remain on the surface (Fig. 4.3b and e) and thus hinder the deposition of further copper at these reaction sites.

In the spray step of the Spray ILGAR process, H_2O is provided by the hydrated $\text{Cu}(\text{hfac})_2 \cdot x \text{H}_2\text{O}$ molecules (Fig. 3.1). Here, the degree x of hydration is $x \leq 1$ [Sigma_2 '08]. Hence, it is likely that in an open system like the Spray ILGAR setup (Fig. 3.3), the

deposition rate is limited by the available amount of H_2O , i.e. by the removal of adsorbed hfac groups (Fig. 4.3b and e). As mentioned in Ref. [Cohen '92], this can lead to a carbon contamination of the deposited copper films and may explain the carbon content of 2 ± 1 at. % of the Spray ILGAR Cu_{2-x}S thin films that was detected by ERDA (section 3.1.4.).

This proposed copper deposition mechanism is only valid for the deposition of copper onto a metal surface. In the Spray ILGAR process the spray step is followed by a H_2S step. Thus, in the spray step of the second ILGAR-cycle, copper is deposited onto a non-metallic surface⁶. Hence, the reduction of $\text{Cu}^{\text{II}}(\text{hfac})_2$ to $\text{Cu}^{\text{I}}\text{hfac}$ and $\cdot\text{hfac}$ has to occur differently (Eq. (4.12a); Fig. 4.3a). It is proposed that on a sulfurized surface, the $\text{Cu}^{\text{II}}(\text{hfac})_2$ reacts with dangling Cu- and S-bonds at the surface, so that $\text{Cu}^{\text{I}}\text{hfac}$ bonds to a dangling bond of a sulfur atom, while the $\cdot\text{hfac}$ radical reacts with a dangling Cu-bond. If this is the case, all following processes (Fig. 4.3b-f) can proceed analogously to the deposition process on a metal surface.

In conclusion, it was shown that under conditions as they are used for the Spray ILGAR deposition of CuInS_2 (Table 3.6), the spraying of a $\text{Cu}(\text{hfac})_2/\text{acetone}$ solution leads to the deposition of metallic copper on the substrate. A mechanism for the copper deposition was proposed, whose rate is limited by the available amount of H_2O , which is provided by the hydrated $\text{Cu}(\text{hfac})_2$ molecules. In this process, the presence of H_2O leads to the removal of adsorbed hfac groups, which otherwise block the reaction sites on the surface for further copper deposition.

4.2.2. Deposition of an Indium-Containing Precursor Compound

In the spray step of the Spray ILGAR deposition process (section 3.3.2.), copper- and indium-containing precursor layers are deposited from a mixed acetone solution of $\text{Cu}(\text{hfac})_2$ and InCl_3 . The identification of the indium-containing precursor compound is the focus of this section. In the Spray ILGAR deposition processes of $\text{In}_2(\text{O,S})_3$ (section 3.2.) and CuInS_2 (section 3.3.2.), In_2O_3 was detected as a secondary phase in both kinds of films (Fig. 3.7 and 3.11a). This indicates that In_2O_3 is the indium-containing phase that is deposited in the spray step of both processes prior to sulfurization. In order to verify this, the deposition process from pure $\text{InCl}_3/\text{acetone}$ solutions in the absence of $\text{Cu}(\text{hfac})_2$ is investigated in this section.

Identification of the Indium-Containing Precursor Compound

A Spray ILGAR deposited thin film was grown (sample 402) by spraying 25 ml of a 40 mM InCl_3 / acetone in repeated spray steps of 30 s (16 spray steps). For comparison, these values are in the same range as those used for the deposition of Spray ILGAR CuInS_2 thin films (Appendix I). In order to identify the indium-containing compound present in this film, the film was investigated by grazing incidence XRD (0.5°).

Fig. 4.4 shows the X-ray diffractogram of this sample. The detected reflections match those of In_2O_3 (JCPDS 00-006-0416). The In_2O_3 is the only detectable phase. This verifies the assumption that the spraying of $\text{InCl}_3/\text{acetone}$ solutions under conditions as they are used for the Spray ILGAR deposition of CuInS_2 thin films (Table 3.6), leads to the deposition of In_2O_3 . It can also be seen from Fig. 4.4 that the relative intensities of diffractogram deviate from those of the reference powder diffractogram. In particular, the intensity ratio of the {222}- and {400}-reflections decreased by a factor of 25 compared to the reference. This indicates that the film is textured in the [001]-direction. This texture is peculiarly characteristic for In_2O_3 thin films, which were deposited by spray pyrolysis using InCl_3 solutions [Ratcheva '86;

⁶ In case of copper sulfide deposition, the surface consists of Cu_{2-x}S (section 3.1.4.). In case of CuInS_2 deposition it consists of Cu_{2-x}S and In_2O_3 (section 4.4.2.3.).

Korotcenkov '02]. The origin of the textured growth mode of In_2O_3 was not studied any further. It will, however, become important that the growth proceeds in a preferential mode (section 4.3.).

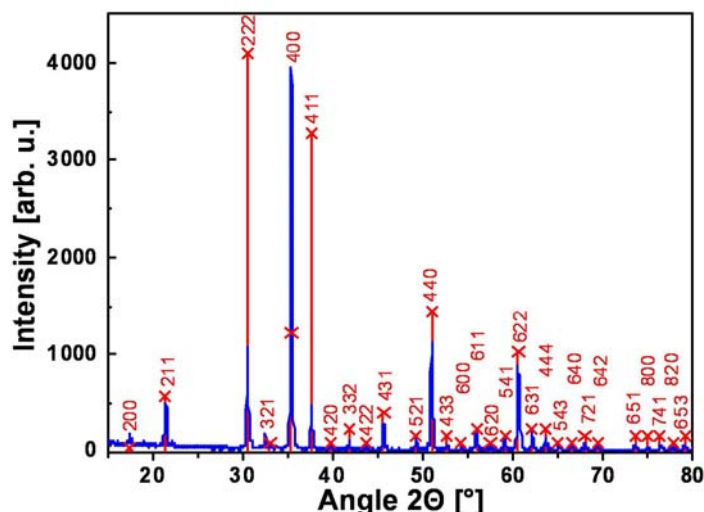


Fig. 4.4: X-ray diffractogram of a thin film (sample 402) deposited by spraying of an InCl_3 /acetone solution under conditions as used for the deposition of Spray ILGAR CuInS_2 thin films (section 3.3.2.; Table 3.6). The reflections are indexed according to a powder reference diffractogram of In_2O_3 (JCPDS-reference 00-006-0416). The diffractogram was obtained by grazing incidence XRD (0.5°).

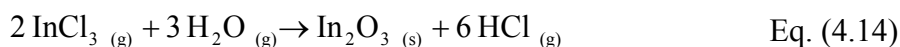
Mechanism of In_2O_3 deposition from InCl_3 /acetone solutions

The first question to be elucidated is the origin of oxygen, which is needed for the formation of In_2O_3 from InCl_3 . Since the deposition took place in an inert nitrogen atmosphere, the formation of In_2O_3 was not expected initially.

Even though high purity acetone (puriss. p.a., $\geq 99.5\%$, Sigma-Aldrich™) was used for the preparation of the spraying solutions, the content of residual water still amounted to a value of $\leq 0.2\%$, as stated by the manufacturer. Thus, for a 40 mM InCl_3 /acetone solution, this corresponds to a total amount of 1 mMol indium and up to 2.8 mMol H_2O for 25 ml of solution ($[\text{In}]:[\text{O}] \geq 0.36$). This means that the residual amount of H_2O in the acetone is already sufficient for the formation of In_2O_3 ($[\text{In}]:[\text{O}] = 0.67$). Furthermore, even the presence of a smaller amount of water, will lead to the partial hydrolysis of InCl_3 and HCl formation. Thus, small amounts of H^+ will initially be present in the solution. This assumption was also verified by testing the pH-value of an InCl_3 /acetone solution with pH-indicators⁷. It is known that small amounts of H^+ can start a catalytic condensation of acetone (CH_3COCH_3) to form H_2O [Coetzee '86; Guthrie '91; Guthrie '92]. The reaction scheme for this condensation process is as follows:



The formation of H_2O during this process leads to further hydrolysis of InCl_3 and thus to an increased H^+ -concentration, so that the reaction rate of Eq. (4.2) further increases. Thus, even if the H_2O content of the acetone should be significantly below the upper limit stated by the manufacturer, it can be expected to increase upon addition of InCl_3 , due to the condensation process in Eq. (4.13). In conclusion, the amount of residual water in the acetone, which was used for the preparation of the spraying solution, was sufficiently high ($\leq 0.2\%$) to propose that the formation of In_2O_3 proceeds by the hydrolysis of InCl_3 (Eq. 4.14):



⁷ The pH-indicators are only calibrated for aqueous solutions. However, by comparing the relative color change of the pH-indicator upon dipping into an InCl_3 /acetone solution, Millipore™ water and pure acetone it was found that the InCl_3 /acetone solution was more acidic (higher H^+ -concentration) than both other liquids.

This also agrees with reports of Asikainen *et al.* [Asikainen '94], who found that the deposition of In_2O_3 by ALD (section 2.2.) also proceeds according to (Eq. (4.14)).

4.2.3. Interactions between the Deposition Processes of Copper and In_2O_3

The identification of the copper- and indium-containing precursor compound, which is deposited in the spray step of the Spray ILGAR deposition process for CuInS_2 thin films, is the focus of this section. It was shown in the previous sections that copper (section 4.2.1.) and In_2O_3 (section 4.2.2.) are deposited, if pure acetone solutions of $\text{Cu}(\text{hfac})_2$ and InCl_3 are respectively used as spraying solutions. Now it is examined how both processes influence each other, if mixed acetone solutions of $\text{Cu}(\text{hfac})_2$ and InCl_3 are used as spraying solutions, as in the Spray ILGAR deposition of CuInS_2 , which was introduced in section 3.3.2.

Bulk Analysis

The bulk analysis of the copper- and indium-containing precursor compounds that are deposited in the spray step of the Spray ILGAR deposition prior to sulfurization was undertaken. The film (sample 403) was prepared by spraying of 45 ml (25 ml of 40 mM $\text{Cu}(\text{hfac})_2/\text{acetone}$ and 20 ml of 40 mM $\text{InCl}_3/\text{acetone}$) in spray steps of 20 s (40 ILGAR-cycles) without any sulfurization. The spray step duration was in the range that was used for the deposition of Spray ILGAR CuInS_2 thin films (Appendix I). The spray steps were separated by breaks of 10 s, in order to avoid continuous cooling of the substrate (section 2.3., page 20). All other parameters were identical to those stated in Table 3.6. A comparable process with a sulfurization step yielded a 743 ± 111 nm thick Spray ILGAR CuInS_2 film (sample 330) in section 3.3.2. Thus, conclusions drawn from the bulk analysis of this sample (sample 403) can be correlated to the processes that occur during the spray step of the Spray ILGAR process.

According to the results presented in sections 4.2.1. and 4.2.2., it was anticipated that this thin film would consist of copper and In_2O_3 , or an intermediate copper- and indium-containing compound like $\text{Cu}_2\text{In}_2\text{O}_5$. ERDA was used to identify the chemical composition of this film (sample 403). Surprisingly, only 2 ± 1 at. % copper, but 33 ± 1 at. % indium, 53 ± 1 at. % oxygen, 6 ± 1 at. % carbon and 3 ± 1 at. % hydrogen were detected in the sample. This composition is close to the composition of In_2O_3 , whilst its copper content is well below the $[\text{Cu}]:[\text{In}]$ ratio of the spraying solution of 1.25.

This result shows that the deposition process that occurs during the spray step of the Spray ILGAR deposition process of CuInS_2 thin films, is more complicated than just a simultaneous deposition of copper and In_2O_3 . In contrast, it was observed in the deposition of the Spray ILGAR CuInS_2 thin films in section 3.3.2. that the $[\text{Cu}]:[\text{In}]$ ratio of the as-deposited films was comparable to that of the spraying solution (Table 3.8). Since the spray step duration determines the amount of precursor material that is deposited prior to sulfurization in every cycle, these results indicate that the $[\text{Cu}]:[\text{In}]$ ratio of the film is influenced by the amount of precursor material that is deposited before the H_2S step of the ILGAR-cycle.

In order to investigate this influence, three Spray ILGAR CuInS_2 thin films were prepared from mixed acetone solutions of $\text{Cu}(\text{hfac})_2$ and InCl_3 ($[\text{Cu}]:[\text{In}] = 1.25$) with spray step durations of 60s, 120 s and 240 s (samples 404-406). For all three films, the same amount of solution (22.5 ml) was sprayed and an H_2S step of 60 s was applied after each spray step in order to reach a complete sulfurization. All other deposition parameters were identical to those listed in Table 3.6. In Fig 4.5, the $[\text{Cu}]:[\text{In}]$ ratios of these films are shown as a function of the spray step duration.

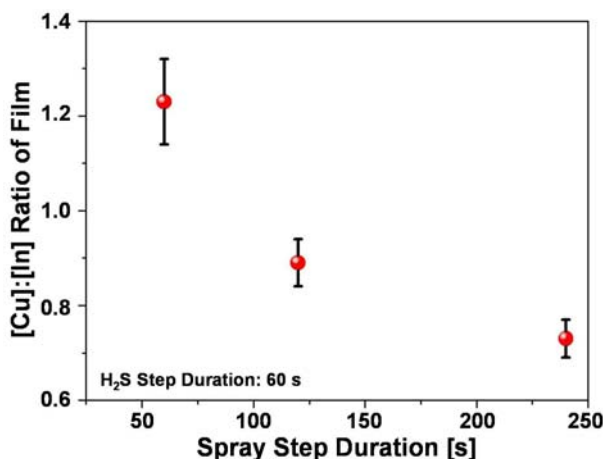


Fig. 4.5: Relation between the [Cu]:[In] ratio of Spray ILGAR CuInS_2 thin films (section 3.3.2.), which have been deposited from mixed acetone solutions of $\text{Cu}(\text{hfac})_2$ and InCl_3 , using spray step durations of 60 s, 120 s and 240 s in every ILGAR-cycle, respectively (sample 404-406). All three films were deposited using the same amount of spraying solution (22.5 ml). The duration of the H_2S step that was applied after every spray step was 60 s. The [Cu]:[In] ratio was measured by XRF. See Appendix I for a detailed list of the preparation parameters.

It can be seen from Fig. 4.5 that the [Cu]:[In] ratio of the deposited Spray ILGAR CuInS_2 thin films decreases for increasing spray step durations. This is strong evidence for an interaction between the deposition processes of copper and In_2O_3 that were observed if pure acetone solutions of $\text{Cu}(\text{hfac})_2$ (section 4.2.1.; sample 401) or InCl_3 (section 4.2.2.; sample 402) were sprayed under comparable conditions. This interaction favors the deposition of In_2O_3 at the expense of copper deposition. The sulfurization in the H_2S step of the ILGAR-cycle (section 4.3.) seems to stop this interaction by converting the deposited phases – or at least their surface – to the corresponding sulfides (Cu_{2-x}S and In_2S_3).

Surface Analysis

In order to study the chemical interaction between the deposition processes of copper and In_2O_3 during the spray step of the Spray ILGAR process, surface-sensitive X-ray Auger spectroscopy (XAS) was applied. Since the energies of Auger transitions are sensitive to the chemical bonds of the respective elements [Moulder '92], this method is well-suited to identify changes in the bonds of copper and indium. Thus, the interaction between the deposition processes of copper and In_2O_3 can be monitored.

In the XAS investigations, a copper- and In_2O_3 -containing layer (deposited from a mixed $\text{Cu}(\text{hfac})_2$ and InCl_3 solution (sample 409)) was compared to pure copper and In_2O_3 layers (deposited from separate $\text{Cu}(\text{hfac})_2$ (sample 407) and InCl_3 solutions (sample 408)). All layers were each prepared in a single spray step (30 s), in order to minimize the loss of copper. All other deposition parameters were identical to those in Table 3.6. The spray step duration of 30 s is a standard value for the Spray ILGAR CuInS_2 deposition process, and thus reflects the conditions during this process.

The spectra of the $\text{InM}_{45}\text{N}_{45}\text{N}_{45}$ and $\text{CuL}_3\text{M}_{45}\text{M}_{45}$ Auger transitions obtained by XAS are shown in Fig. 4.6a and b. The energies of the $\text{InM}_4\text{N}_{45}\text{N}_{45}$ and $\text{InM}_5\text{N}_{45}\text{N}_{45}$ Auger transitions of the In_2O_3 layer and of the copper- and In_2O_3 -containing layer in Fig. 4.6a are identical within the energetic resolution of ± 0.1 eV of the measurements. The only observable difference between both spectra is the onset of the $\text{Cu}2s$ peak in the spectra of the copper-containing layer (Sample 409). In order to verify that this difference in the spectral shape is solely due to the contribution of the $\text{Cu}2s$ peak, the difference spectrum of both spectra (\odot) was fitted by a peak (red trace in Fig. 4.6a), which was centered at the energetic position of the $\text{Cu}2s$ peak ($E_{\text{kin}} = 389$ eV; $E_{\text{bin}} = 1097$ eV; [Moulder '92]). The difference spectrum can be approximated well by such a peak. This indicates that the bonds of the indium atoms in the In_2O_3 and in the copper- and In_2O_3 -containing layers are identical. Thus, the deposition of In_2O_3 seems not to be affected by the presence of $\text{Cu}(\text{hfac})_2$ in the spraying solution.

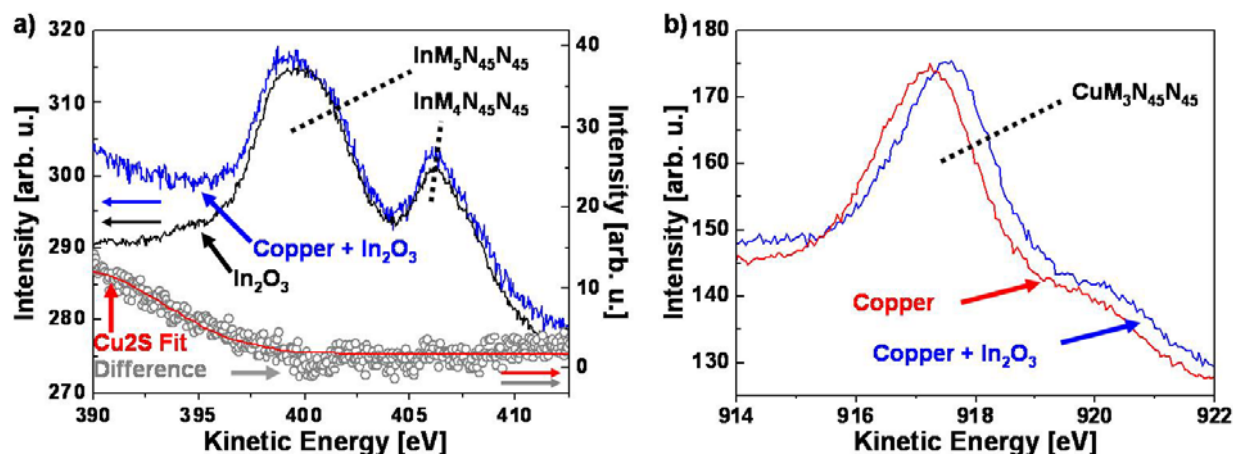


Fig. 4.6: Auger-spectra of the $\text{InM}_{4.5}\text{N}_{4.5}\text{M}_{4.5}$ (a) and $\text{CuL}_3\text{M}_{4.5}\text{M}_{4.5}$ (b) Auger transitions as obtained by XAS from copper (sample 407), In_2O_3 (sample 408) and copper- and In_2O_3 -containing layers (sample 409). In a) the difference spectrum (\circ) of the $\text{InM}_{4.5}\text{N}_{4.5}\text{M}_{4.5}$ spectra was fitted (red trace) in order to approximate the contribution of the $\text{Cu}2s$ peak in the copper-containing layer (sample 409). An $\text{AlK}\alpha$ X-ray source was used for excitation (1486.6 eV). The preparation parameters are listed in Appendix I. The spectra are shifted on the intensity scale for the sake of clarity.

In contrast, a difference in the energies of the $\text{CuL}_3\text{M}_{4.5}\text{M}_{4.5}$ Auger transitions of about 0.3 eV can be observed between spectra obtained from the copper and from the copper- and In_2O_3 -containing layers (Fig. 4.6b). This means that the copper atoms are bound differently in the copper layer and in the copper- and indium-containing layer. However, the Auger transition energies of the $\text{CuL}_3\text{M}_{4.5}\text{M}_{4.5}$ spectra could not be assigned unambiguously to an exact copper compound. Nevertheless, it can be concluded from these measurements that the deposition process of copper is altered by the presence of InCl_3 in the spraying solution (sample 409) compared to the deposition from a pure $\text{Cu}(\text{hfac})_2$ solution. Since XAS only probes the upmost atomic monolayers of the investigated surface, these results show that especially the bonds of the surface copper atoms are altered. These altered copper bonds maybe a key to understanding the decrease of the $[\text{Cu}]:[\text{In}]$ ratio of the deposited films that was observed for increasing spray step durations (Fig. 4.5). Information about how the spray step duration is correlated to the alteration of the copper bonds may be obtained from monitoring the growth of the deposited layers microscopically.

In Fig. 4.7, a plan-view SEM image of a copper- and In_2O_3 -containing layer (sample 410) is shown, which was prepared identically to the one that was investigated by XAS (sample 409; Appendix I) in a single spray step of 30 s.

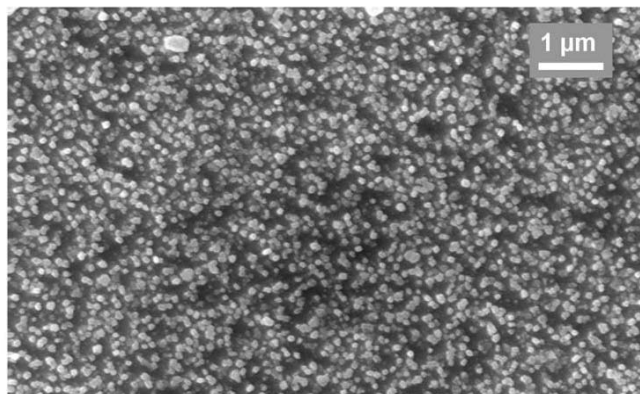


Fig. 4.7: Plan-view SEM image of a copper- and In_2O_3 -containing layer (sample 410), which was deposited in a single spray step of 30 s from a mixed acetone solution of $\text{Cu}(\text{hfac})_2$ and InCl_3 . The preparation parameters were identical to those of the copper- and In_2O_3 -containing layer (sample 409) that was investigated by XAS (Fig. 4.6). See Appendix I for further details.

It can be seen that the deposited layer is not yet closed after 30 seconds of spraying, but the grains are already in contact with each other at many sites. This may explain why the interaction between the deposition processes of copper and In_2O_3 , i.e. the decrease of the $[\text{Cu}]:[\text{In}]$ ratio, becomes more pronounced for increasing spray step durations: For short spray

step durations (< 30 s) the deposited grains are not yet in contact with each other. Therefore, the newly deposited material can still be deposited onto the free surface of the substrate. As the spray step duration increases, the coverage of the substrate increases. Thus, more newly deposited grains will be deposited on top of previously deposited grains. Since the XAS investigations showed that the presence of InCl_3 in the spraying solution leads to an alteration of the bonds of the upmost copper atoms, it can be expected that this alteration of the surface will only start to influence the deposition rate, if the newly deposited material is deposited onto this altered already covered surface. In the following, a possible mechanism for the interaction between the deposition processes of copper and In_2O_3 is proposed.

Interaction between the Deposition Processes of Copper and In_2O_3 : The Role of H_2O

A mechanism for the interaction between the deposition processes of copper and In_2O_3 during the spray step of the Spray ILGAR deposition process for CuInS_2 thin films is proposed in the following, which can explain the observed dependence of the $[\text{Cu}]:[\text{In}]$ ratio of the deposited layer on the duration of the spray step. This mechanism is depicted in Fig. 4.8a-b.

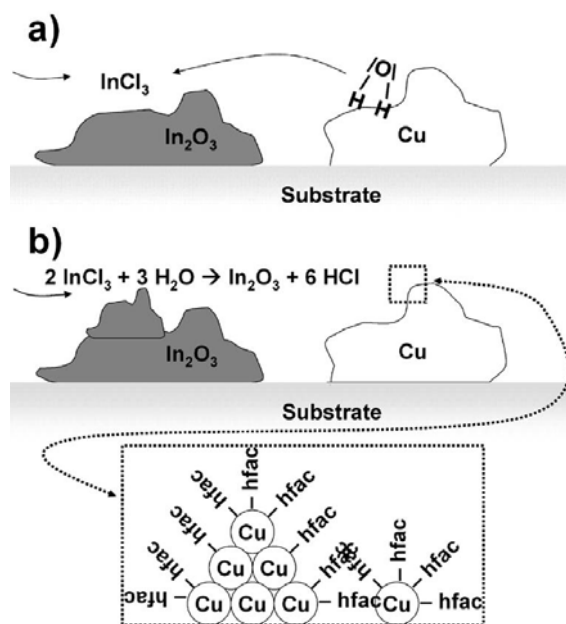


Fig. 4.8: Schematic sketch of the proposed interaction between the deposition processes of copper and In_2O_3 during the spray step of the Spray ILGAR deposition process for CuInS_2 thin films. During the spray step, both processes compete for the limited amount of H_2O in the solution. Since H_2O is consumed in the In_2O_3 deposition process, but only acts catalytically in the copper deposition process, H_2O will be consumed by the hydrolysis of InCl_3 on the expense of copper deposition (a). This prevents the removal of hfac groups from the deposited copper grains and thus hinders further copper deposition by blocking deposition sites (b).

It was shown in the previous sections that H_2O plays a key role in the deposition process of copper (section 4.2.1.) as well as in that of In_2O_3 (section 4.2.2.): In the In_2O_3 deposition process, H_2O is consumed by the hydrolysis of InCl_3 (Eq. (4.14)), while in the deposition process of copper, it acts catalytically and is released at the end of the process (Fig. 4.3b, c, e, f). Note that all H_2O in the spraying solution either stems from the hydrated $\text{Cu}(\text{hfac})_2$ compound or from impurity H_2O in acetone (partially increased by the condensation reaction, described in Eq. (4.13)). Hence, only small amounts of H_2O (some mMol in 25 ml of solution) are available in the solution. Thus, the deposition processes of copper and In_2O_3 compete for this limited amount of H_2O during the spray step. Thereby, also H_2O , stemming from $\text{Cu}(\text{hfac})_2$ is consumed by the hydrolysis process of InCl_3 (Fig. 4.8a). This will lead to a decrease of the copper deposition rate, since firstly, the adsorbed Cu^{hfac} species cannot be converted to Cu_2O and secondly, the adsorbed $\cdot\text{hfac}$ radicals cannot be removed from the surface (Fig. 4.3b, c, e, f). At the same time, the deposition rate for In_2O_3 will increase, since more H_2O (stemming from the hydrated $\text{Cu}(\text{hfac})_2$) is available (Fig. 4.8b). As long as the substrate is not covered completely by grains of copper and In_2O_3 , the lack of H_2O in the copper deposition process will not affect the deposition rate of copper (Eq. (4.12a)), since there will still be free deposition sites on the surface, at which this process can occur.

However, already at this stage the lack of H₂O will prevent the removal of the hfac groups. This is likely the reason, why in Fig. 4.6b, a shift in the CuL₃M₄₅M₄₅ spectrum was observed upon the presence of InCl₃. As soon as the substrate is covered completely (spray step duration > 30 s; Fig. 4.8), further copper or In₂O₃ can only be deposited on top of previously deposited copper or In₂O₃ grains. Thereby it can be expected that on top of an In₂O₃ grain the deposition of In₂O₃ will be favored compared to that of copper. Due to the lack of H₂O, the surface of the previously deposited copper grains will be covered by adsorbed hfac groups. Therefore, the charge transfer step in Eq. (4.12a), which is needed for the deposition of copper cannot occur, since no free electrons (from a metal surface or a dangling bond) are available. Hence as soon, as the substrate surface is completely covered by In₂O₃ and copper, the copper deposition rate can be expected to decrease, as it was observed in Fig. 4.5⁸. Furthermore, the lack of H₂O can also explain the high carbon content of 6 ± 1 at. % in the unsulfurized copper- and In₂O₃-containing thin film (sample 403; p. 57) by the incorporation of adsorbed hfac groups into the film matrix.

Test of the Proposed Mechanism: The Addition of H₂O

According to the proposed mechanism for the interaction between the deposition processes of copper and In₂O₃, the addition of H₂O to the spraying solution should lead to an increase of the copper deposition rate, since more H₂O is available. In order to verify this, another unsulfurized copper- and In₂O₃ thin film (sample 411) was deposited from a mixed acetone solution of Cu(hfac)₂ and InCl₃ under identical conditions as the previously investigated film (sample 403; p. 57). The only difference being, that 2 ml of Millipore™ H₂O (about 100 mMol of H₂O) were added to the spraying solution of sample 411, which roughly corresponds to a twentyfold increase of the H₂O content of the spraying solution. In order to test the validity of the proposed mechanism, the [Cu]:[In] ratios of both films were compared by measuring the count rates of the X-ray lines of copper and indium (CuK_α, CuL_α, InK_α, InL_α) of both films (samples 403, 411) by XRF. The XRF-count rates are listed in Table 4.1⁹.

Table 4.1: XRF-count rates for copper- and In₂O₃-containing thin films, which were deposited with and without the addition of H₂O (2 ml) from a mixed acetone solution (45 ml) of Cu(hfac)₂ and InCl₃ under identical conditions. See Appendix I for preparation parameters.

	Without H ₂ O (sample 403)	H ₂ O added (sample 411)
CuK _α [counts/s]	7.8 ± 0.1	55.0 ± 0.1
CuL _α [counts/s]	10.2 ± 0.1	70.2 ± 0.1
InK _α [counts/s]	175.5 ± 0.1	77.4 ± 0.1
InL _α [counts/s]	617.7 ± 0.1	294.9 ± 0.1

The addition of H₂O led to a sevenfold increase of the CuK_α and CuL_α count rates. At the same time, the indium signal decreased by a factor of two. The latter may be due to a reduced spray-rate, which was observed upon the addition of H₂O to the spraying solution¹⁰. However, the [Cu]:[In] ratio of the deposited film is clearly shifted towards higher copper contents by the addition of H₂O, which reveals the influence of H₂O on the deposition process of copper and thus helps validate the proposed mechanism.

In conclusion, the results of this section (section 4.2.) showed that the precursor layer, which is deposited in the spray step of the Spray ILGAR deposition process of CuInS₂ thin films, consists of copper and In₂O₃. The observed influence of the spray step duration on the [Cu]:[In] ratio of the deposited precursor layer could be explained by the limited amount of

⁸ The influence of the H₂S step on the [Cu]:[In] ratio of the deposited film is discussed in section 4.3.

⁹ Since the XRF-calibration was not valid for copper- and In₂O₃-containing films, no absolute values for the [Cu]:[In] ratio of the deposited films were determined.

¹⁰ The reduced spray-rate for sample 411 is due to the properties of H₂O and acetone (Table 3.3; section 3.1.3.).

H₂O in the spraying solution. Due to the consumption of H₂O by the hydrolysis of InCl₃, not enough H₂O is left for the removal of adsorbed hfac groups from the deposited copper, which hinders further copper deposition and favors the incorporation of carbon into the film.

4.3. Precursor Layer Sulfurization

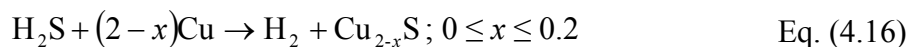
The previously discussed copper and In₂O₃ thin films were deposited without sulfurizing. The films discussed and analyzed in this section are grown with the sulfurizing H₂S step of the ILGAR-cycle. Thereby, the processes occurring during the sulfurization process are focused. In the Spray ILGAR deposition processes of Cu_{2-x}S (0 ≤ x ≤ 0.2; section 3.1.4.) and In₂(O,S)₃ (section 3.2.) thin films, copper and In₂O₃ are deposited as precursor compounds prior to the H₂S step because these films were deposited under identical conditions as the layers analyzed in sections 4.2.1 and 4.2.2. Thus, it can be concluded that copper and In₂O₃ are converted to Cu_{2-x}S and In₂(O,S)₃ during the H₂S step of the ILGAR-cycle, if only one of these compounds is present. If both compounds (copper and In₂O₃) are sulfurized simultaneously, as in the Spray ILGAR process for CuInS₂ thin films, CuInS₂ is formed additionally (section 3.3.2.). The diffusion processes that lead to the formation of Cu_{2-x}S, In₂(O,S)₃ and CuInS₂ during the H₂S step, are discussed in the following. In particular, this discussion will reveal why copper is sulfurized completely, whereas the sulfurization of In₂O₃ is incomplete. The values for the diffusion coefficients that are used in this section are summarized in Appendix V in Table V.1 and Fig. V.1.

Copper Sulfide Formation

During the H₂S step of the ILGAR-cycle, the previously spray-deposited copper is converted to a blend of β-Cu₂S (α-Cu₂S at room temperature), and the digenite phases Cu_{1.81}S and Cu₉S₅ (Fig. 3.5). The characterization of Spray ILGAR Cu_{2-x}S (0 ≤ x ≤ 0.2; section 3.1.4.) did not indicate the presence of unsulfurized copper in these films. Thus, it can be assumed that all copper, which was deposited in the spray step of the ILGAR-cycle, is sulfurized to Cu_{2-x}S in the H₂S step. The coexistence of the three copper sulfide phases is likely due to the phase transition of β-Cu₂S to digenite Cu_{2-δ}S and copper, which occurs at 437 °C [Landolt '08]:



The transition temperature of this phase transition is close to the substrate temperature of the Spray ILGAR process of 430 °C and is thus likely to occur during the process. The copper, which is given off in this phase transformation, will react with H₂S to form further Cu_{2-δ}S. During the cooling of the sample after the deposition process, some of the digenite phases will be firstly converted to β-Cu₂S, which then becomes α-Cu₂S for temperatures below 103 °C (section 2.1.3.). However, since the digenite phases are copper-poor compared to α-Cu₂S and β-Cu₂S, not enough copper is present in the film for a complete conversion of digenite Cu_{2-δ}S to α-Cu₂S and β-Cu₂S. Thus, some digenite will remain in the film. This assumption is further supported by the fact that the observed digenite phases Cu_{1.81}S and Cu₉S₅ belong to the digenite phases with the lowest copper content (Fig. IV.1; Table 2.2). In general, the sulfurization of copper to a copper sulfide compound of the composition Cu_{2-x}S (0 ≤ x ≤ 0.2) can be described by the following equation:



If copper is present as a grain in a polycrystalline film, this reaction will firstly only occur at the surface of the grain. After the complete sulfurization of the grain surface, no direct reaction between copper and H₂S according to Eq. (4.16) is possible anymore, since both phases are separated by a surface layer of Cu_{2-x}S. Thus, the sulfurization can only proceed by

the diffusion of copper (or sulfur) through the Cu_{2-x}S surface layer. Using a formula derived by Bartkowicz *et al.* [Bartkowicz '86] for the diffusion of copper in Cu_2S , the self-diffusion coefficient of copper at 430 °C can be calculated to $D_{\text{Cu}_{2\text{S}}}^{\text{Cu}} = 1.9 \cdot 10^{-5} \text{ cm}^2 \text{ s}^{-1}$. According to Eq. (4.11), the diffusion length of copper in $\beta\text{-Cu}_2\text{S}$ during a typical H_2S step of 20 s (section 3.1.3; Table 3.6), can be calculated as $L_{D_{\text{Cu}_{2\text{S}}}^{\text{Cu}}} \approx \sqrt{D_{\text{Cu}_{2\text{S}}}^{\text{Cu}} \cdot \Delta t_{\text{H}_2\text{S}}} \approx 600 \text{ }\mu\text{m}$. This exceeds the size of the copper grains ($< 100 \text{ nm}$; Fig. 4.7), which are deposited during the spray step, by several orders of magnitude. According to Ref. [Price '81; Pauporte '99], the self-diffusion coefficient of copper in the digenite phase (including Cu_9S_5 and $\text{Cu}_{1.81}\text{S}$) is in the same range as that of $\beta\text{-Cu}_2\text{S}$ as it can be seen from Table V.1 in Appendix V. Thus, for all observed Cu_{2-x}S phases, the copper diffusion length for a H_2S step duration of 20 s exceeds the size of the deposited copper grains. Consequently, after the sulfurization of the upmost atomic layers of a copper grain, copper can completely diffuse through the newly formed Cu_{2-x}S to reach the grain surface where it reacts to further Cu_{2-x}S with H_2S . Thereby the entire grain will be sulfurized progressively.

The self-diffusion coefficient of sulfur in copper sulfides is five to six orders of magnitudes smaller than that of copper [Blachnik '01]. Hence, the sulfurization of copper by the diffusion of sulfur into the grain after a decomposition of H_2S can be neglected.

From these kinetic considerations, the complete sulfurization of copper to Cu_{2-x}S during the H_2S step of the Spray-ILGAR process can be explained by the fast diffusion of copper in Cu_{2-x}S phases to the grain surface, where it is converted to Cu_{2-x}S by reacting with H_2S .

Formation of $\text{In}_2(\text{O},\text{S})_3$

In contrast to the sulfurization of copper, the sulfurization of In_2O_3 during the H_2S step of the ILGAR-cycle was found to be incomplete, in both the Spray ILGAR $\text{In}_2(\text{O},\text{S})_3$ (section 3.2.; Fig. 3.7) and CuInS_2 thin films (3.3.2.; Fig. 3.11a). The origin of this incomplete sulfurization is discussed in the following.

The characterization of an Spray ILGAR $\text{In}_2(\text{O},\text{S})_3$ thin film (sample 324) by XRD, ERDA and SEM in section 3.2. revealed that the film consisted of In_2S_3 and In_2O_3 with an integral composition of $37 \pm 1 \text{ at. } \%$ indium, $34 \pm 1 \text{ at. } \%$ oxygen, $25 \pm 1 \text{ at. } \%$ sulfur, $2 \pm 1 \text{ at. } \%$ hydrogen and $1 \pm 1 \text{ at. } \%$ chlorine. The film was also found to be highly structured (Fig. 3.8). An ERDA composition depth-profile of this film is shown in Fig. 4.9a.

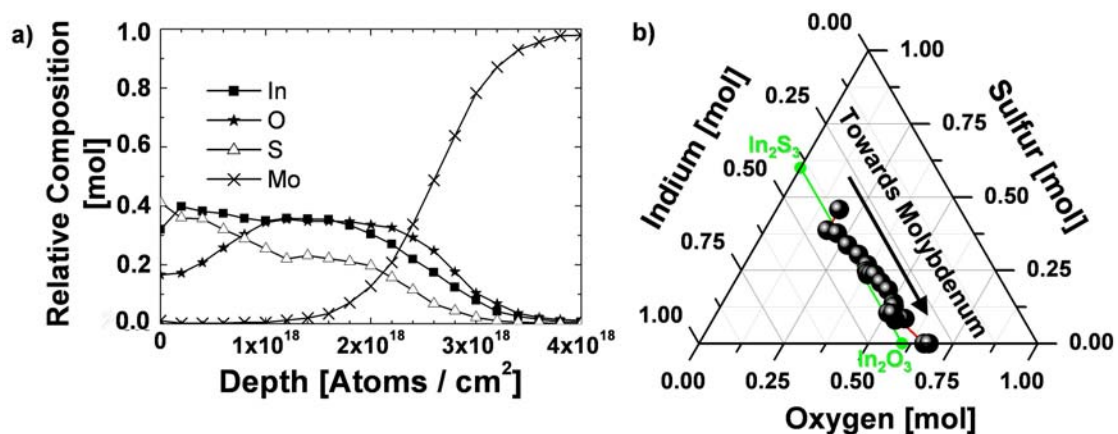


Fig. 4.9: a) ERDA depth profile of a Spray ILGAR $\text{In}_2(\text{O},\text{S})_3$ thin film (sample 324) for the most prominent elements indium, oxygen, sulfur and molybdenum. Additionally, $2 \pm 1 \text{ at. } \%$ hydrogen and $1 \pm 1 \text{ at. } \%$ chlorine were detected. b) Ternary composition diagram of the relative molar amounts of indium, sulfur and oxygen in this film, as calculated from the depth-profile in a). Additionally, the $\text{In}_2\text{S}_3\text{-In}_2\text{O}_3$ tie-line is indicated (green line). The arrow in b) indicates the direction of increasing depth in the film. The size of spots accounts for the uncertainties of $\pm 0.02 \text{ mol}$.

The gradient in the [In]:[O]:[S] ratio is overlaid by the increasing contribution of the molybdenum signal of the substrate in Fig. 4.9a¹¹. For clarity, the [In]:[O]:[S] ratio in the film between its surface and the molybdenum substrate is depicted in Fig. 4.9b in form of a ternary composition diagram, calculated from the data in Fig. 4.9a. The In₂O₃-In₂S₃ tie line is marked in Fig. 4.9b by the green line as a reference. Apparently, the [In]:[O]:[S] ratio of the film evolves closely along the In₂O₃-In₂S₃ tie line between the molybdenum substrate and the film surface. The sulfur content of the film continuously decreases from 46 ± 2 at. % at the film surfaces to zero at the molybdenum layer.

The material at the molybdenum layer was deposited in the first ILGAR-cycle and was thus present during all following cycles and their H₂S steps, whereas the upmost sulfur-rich part of the film was deposited in the last ILGAR-cycle of the process and was only sulfurized during one H₂S step. Hence, for the case of incomplete sulfurization, one would intuitively expect that the film shows the lowest sulfur content at its surface, which then increases towards the molybdenum layer. That the opposite observation is made can be understood, if the structural properties of the film are taken into account. A comparison of the X-ray diffractograms of the In₂(O,S)₃ (sample 324; Fig. 3.7) and In₂O₃ (sample 404; Fig. 4.4) thin films reveals that the intensity ratio of the In₂O₃ {222}- and {400}-reflections for the In₂(O,S)₃ thin films corresponds to that of the powder reference (Fig. 3.7), whereas the pure In₂O₃ thin film, which was investigated in section 4.2.2., was textured in the [001]-direction (Fig. 4.4.; section 4.2.2.). This shows that the sulfurization of In₂O₃ in the H₂S step prevents the preferential growth of In₂O₃. This is presumably due to the fact that the sulfurization changes the crystallographic structure of the In₂O₃ surface. Thus, the In₂O₃, which is deposited in the following spray step, will grow on an In₂S₃ surface instead of an In₂O₃ surface. Since the crystal structures of both compounds are different (section 2.1.3), the growth of In₂O₃ will not proceed preferentially as in the unsulfurized case.

Additionally, the SEM-image of the In₂(O,S)₃ thin film in Fig. 3.8 shows that the upper part of the film (sulfur-rich) is highly structured, whilst the lower part is compact.

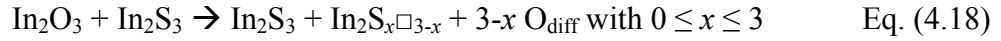
These observations indicate that the prevention of the preferential growth of In₂O₃ by the sulfurization during the H₂S step results in a structured growth mode. Thus, it may be assumed that the surface area of the film continuously increases from one ILGAR-cycle to the next. If the sulfurization of In₂O₃ by H₂S is diffusion-limited, such an increase in the surface area would result in an increasing sulfur content of the film at the film surface, due to the increased contact area between H₂S and In₂O₃.

In order to estimate the amount of In₂O₃ that is converted to In₂S₃ in the H₂S step, the sulfurization reaction and the corresponding diffusion processes are discussed in the following. The conversion of In₂O₃ to In₂S₃ by H₂S occurs via the following equation:

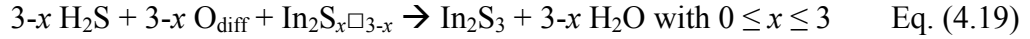


This reaction can only occur at a freely accessible surface, since not only must the H₂S molecules be able to reach the reaction site, but also the H₂O-molecules must be able to leave it. This means that after the conversion of the upmost atomic layers of In₂O₃ to In₂S₃, the reaction described in Eq. (4.17) will stop, since H₂S and In₂O₃ are separated by an In₂S₃ surface layer. In the following, a further sulfurization is only possible, if sulfur and oxygen are exchanged by diffusion through the In₂S₃ layer. Since the In₂S₃ layer contains sulfur, it can be assumed that the sulfurization rate is limited by the diffusion rate of oxygen through the In₂S₃ layer. This process may be described by the reaction in Eq. (4.18), where □ denotes a sulfur vacancy in the In₂S₃ lattice:

¹¹ The overlap of the molybdenum signal with those of indium, oxygen and sulfur in Fig. 4.9a results from the rough surface morphology of the probed film (Fig. 3.8). A real interdiffusion across the Mo/In₂(O,S)₃ interface can be excluded from complimentary SEM/EDX measurements. For a detailed discussion of roughness effects in ERDA measurements, the reader is referred to Ref. [Lindner '03].



Initially, sulfur and oxygen ions will interdiffuse across the $\text{In}_2\text{O}_3/\text{In}_2\text{S}_3$ interface. This process can be described as a conversion of In_2O_3 to In_2S_3 by the indiffusion of sulfur into the In_2O_3 grain. This leads to the formation of sulfur vacancies in the In_2S_3 layer and the indiffusion of oxygen into this layer (O_{diff}). Depending on the diffusion coefficient of oxygen in In_2S_3 , the indiffused oxygen, will either occupy the sulfur vacancies or diffuse further towards the surface to react with H_2S according to Eq. (4.19):



The diffusion of oxygen in In_2S_3 has not been investigated. However, some conclusions about this process can be drawn from the diffusion of sulfur in In_2S_3 and of oxygen in In_2O_3 . These processes were studied in tracer diffusion experiments of the radioisotopes ^{35}S and ^{18}O by Tezlevan *et al.* [Tezlevan '93] and Ikuma *et al.* [Ikuma '96; Ikuma '98], respectively. Tezlevan *et al.* determined the frequency factor and the activation energy for the diffusion of sulfur in single-crystalline (sc) In_2S_3 as $D_0^{\text{S-sc-In}_2\text{S}_3} = 134.2 \text{ cm}^2\text{s}^{-1}$ and $E_A^{\text{S-sc-In}_2\text{S}_3} = 1.5 \text{ eV}$ [Tezlevan '93]. For the diffusion of oxygen, Ikuma *et al.* determined values of $D_0^{\text{O-sc-In}_2\text{O}_3} = 7.4 \cdot 10^5 \text{ cm}^2\text{s}^{-1}$ and $E_A^{\text{O-sc-In}_2\text{O}_3} = 6.1 \text{ eV}$ in single-crystalline In_2O_3 [Ikuma '98] and of $D_0^{\text{O-pc-In}_2\text{O}_3} = 5.2 \cdot 10^5 \text{ cm}^2\text{s}^{-1}$ and $E_A^{\text{O-pc-In}_2\text{O}_3} = 5.1 \text{ eV}$ in polycrystalline (pc) In_2O_3 [Ikuma '96]. At 430 °C in the Spray ILGAR process, this corresponds to diffusion coefficients of $D^{\text{S-sc-In}_2\text{S}_3} = 2.0 \cdot 10^{-9} \text{ cm}^2\text{s}^{-1}$ for the diffusion of sulfur in sc- In_2S_3 , $D^{\text{O-sc-In}_2\text{O}_3} = 1.0 \cdot 10^{-39} \text{ cm}^2\text{s}^{-1}$ for the diffusion of oxygen in sc- In_2O_3 and $D^{\text{O-pc-In}_2\text{O}_3} = 1.7 \cdot 10^{-29} \text{ cm}^2\text{s}^{-1}$ for the diffusion of oxygen in pc- In_2O_3 . These values show that the diffusion of oxygen in In_2O_3 is much slower (20-30 orders of magnitude) than that of sulfur in In_2S_3 . From a crystallographic point of view this is surprising, since in the cubic lattice of In_2O_3 , two oxygen vacancies exist in the direct neighborhood of every cation [Marezio '66], whereas in the spinel In_2S_3 only cation vacancies exist (section 2.1.3.). Therefore, the diffusion of the anion oxygen in In_2O_3 would be expected to proceed faster than that of sulfur in In_2S_3 . This is also reflected by the higher frequency factor of the oxygen diffusion in In_2O_3 compared to that of sulfur diffusion in In_2S_3 , which corresponds to the diffusion coefficient at infinite temperature (Eq. (4.5)). That the opposite phenomenon is observed, indicates that the In-O bond in In_2O_3 is much stronger than the In-S bond in In_2S_3 , which can be seen from a comparison of the activation energies of both diffusion processes, as well as of the enthalpies of formation of In_2O_3 ($\Delta G_{\text{In}_2\text{O}_3}(427 \text{ °C}) = -879222 \text{ Jmol}^{-1}$) and of In_2S_3 ($\Delta G_{\text{In}_2\text{S}_3}(427 \text{ °C}) = -289929 \text{ Jmol}^{-1}$; Appendix X). Therefore, at the temperatures used in the ILGAR process, the strong In-O bond hinders the fast diffusion of oxygen in In_2O_3 . Hence, for the diffusion of oxygen in In_2S_3 , the activation energy can be expected to exceed the activation energy for sulfur diffusion in In_2S_3 . However, the cation vacancies in the In_2S_3 lattice lead to the assumption that the activation energy for oxygen diffusion in In_2S_3 is lower than that for oxygen diffusion in In_2O_3 , thus:

$$5.1 \text{ eV} = E_A^{\text{O-pc-In}_2\text{O}_3} > E_A^{\text{O-In}_2\text{S}_3} > E_A^{\text{S-sc-In}_2\text{S}_3} = 1.5 \text{ eV} \quad \text{Eq. (4.20)}$$

At a temperature of 430 °C the oxygen diffusion in In_2S_3 can be expected to proceed slower than the sulfur diffusion in In_2S_3 and faster than the oxygen diffusion in In_2O_3 . The diffusion length for the sulfur diffusion in In_2S_3 at 430 °C can be calculated according to Eq. (4.11) as $L_{D^{\text{S-In}_2\text{S}_3}} \approx \sqrt{D^{\text{S-In}_2\text{S}_3} \cdot \Delta t_{\text{H}_2\text{S}}} \approx 2 \text{ }\mu\text{m}$, whereas for the diffusion of oxygen in In_2O_3 , the *calculated* diffusion length is below 1 Å. This is less than the average length of the In-O bond in In_2O_3 of 2.18 Å [Marezio '66] and merely shows that this diffusion process is negligible at 430 °C. In Fig. 4.10, the diffusion coefficients of sulfur in sc- In_2S_3 [Tezlevan '93], of oxygen in pc- In_2O_3 [Ikuma '96] and of oxygen in sc- In_2O_3 [Ikuma '98] are shown as a function of temperature.

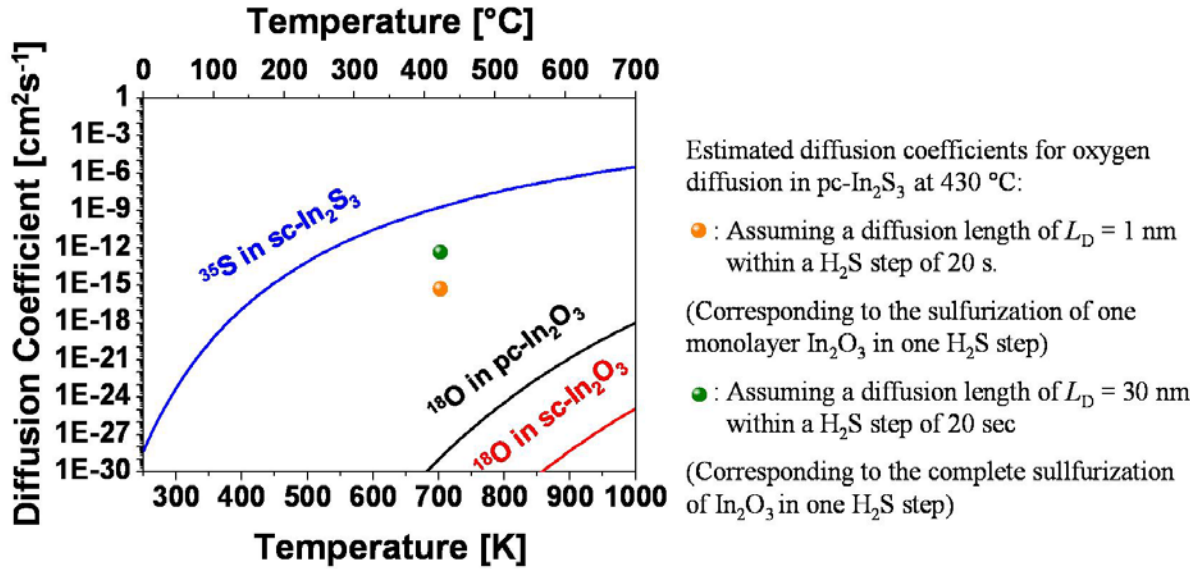


Fig. 4.10: Temperature-dependent diffusion coefficients for the diffusion of sulfur in sc-In₂S₃, oxygen in pc-In₂O₃ and oxygen in sc-In₂O₃ after Ref. [Tezlevan '93], [Ikuma '96] and [Ikuma '98], respectively. Additionally, the diffusion coefficient for the diffusion of oxygen in In₂S₃ is estimated, based on the assumptions that 1 nm of In₂O₃ (orange) or 30 nm of In₂O₃ (green) are sulfurized during a H₂S step of 20 s in the Spray ILGAR process for In₂(S,O)₃ thin films. Thereby, the thickness of the sulfurized layer was approximated by the diffusion length of oxygen in In₂S₃ according to Eq. (4.11). The frequency factors and activation energies for these diffusion processes are summarized in Table V.1 and Fig. V.1 in Appendix V.

Additionally, two estimated values for the diffusion coefficient for the diffusion of oxygen in In₂S₃ are shown, which result from the assumptions that either 1 nm of In₂O₃ (orange) or 30 nm of In₂O₃ (green) are fully sulfurized during a 20 s exposure to H₂S. The thickness of the sulfurized layer was approximated by the diffusion length of oxygen in In₂S₃ according to Eq. (4.11). A sulfurization of 1 nm corresponds to the sulfurization of the upmost In₂O₃ monolayer of the In₂O₃ grain (the length of the unit cell of In₂O₃ is $a = 10.117 \pm 0.001 \text{ \AA}$ [Marezio '66]) and can be understood as the limiting case of the sulfurization as a pure surface reaction. The sulfurization of 30 nm of In₂O₃ corresponds to the complete sulfurization of all In₂O₃ that was deposited in the previous spray step. Since in the Spray ILGAR process of In₂(O,S)₃ (sample 324), the sulfurization was found to be incomplete, the actual diffusion coefficient for oxygen diffusion in In₂S₃ can be assumed to lie in between these values. In a first approximation, it may be assumed that the frequency factor for the oxygen diffusion is determined by the lattice of In₂S₃, whereas the activation energy follows from the strength of the In-O bond. Then $D_0^{\text{O}}_{\text{In}_2\text{S}_3} \approx D_0^{\text{S}}_{\text{sc-In}_2\text{S}_3} = 134.2 \text{ cm}^2\text{s}^{-1}$ can be assumed and the activation energy for oxygen diffusion in In₂S₃ can be estimated according to Eq. (4.7) as:

$$E_A^{\text{O}}_{\text{In}_2\text{S}_3} \approx -0.06 \cdot \ln \left(\frac{D(T = 430^\circ\text{C})}{D_0^{\text{S}}_{\text{sc-In}_2\text{S}_3}} \right) \quad \text{Eq. (4.21)}$$

For the upper limit of an oxygen diffusion length of 30 nm (complete sulfurization) Eq. (4.21) yields an activation energy of $E_A^{\text{O}}_{\text{In}_2\text{S}_3} \approx 2.0 \text{ eV}$, whereas for a diffusion length of 1 nm, an activation energy of $E_A^{\text{O}}_{\text{In}_2\text{S}_3} \approx 2.4 \text{ eV}$ follows. From this approximation, the activation energy of the diffusion process of oxygen can be estimated as:

$$2.4 \text{ eV} > E_A^{\text{O}}_{\text{In}_2\text{S}_3} \geq 2.0 \text{ eV} \quad \text{Eq. (4.22)}$$

This is in agreement with Eq. (4.20) and corresponds to a ratio of the activation energies for the diffusion processes of oxygen and sulfur in In₂S₃ of $0.63 < E_A^{\text{S}}_{\text{sc-In}_2\text{S}_3} / E_A^{\text{O}}_{\text{In}_2\text{S}_3} \leq 0.76$. Based

on the above considerations about the interaction of the diffusing sulfur or oxygen atoms with the In_2S_3 lattice, the estimated range of the activation energy seems reasonable. Additionally, the activation energy of the diffusion of sulfur and oxygen in In_2S_3 can be assumed to depend on the electronegativities of both atoms (2.58 for sulfur, 3.44 for oxygen on Pauling scale [www_6 '08]). The ratio of the electronegativities of sulfur and oxygen is about 0.75 and lies in the same range as the ratio of both activation energies and thus supports the assumption made in this discussion.

The incomplete In_2O_3 sulfurization in the Spray ILGAR deposition can thus be explained: An In_2S_3 surface layer rapidly forms on the In_2O_3 grains. The slow diffusion of oxygen through this initial In_2S_3 surface layer hinders full In_2S_3 conversion of the In_2O_3 grains during the H_2S step of the ILGAR-cycle. The increase of the sulfur content towards the film surface that was observed in Fig. 4.9b can be explained by the increase of the surface area of the film with every cycle. The latter is assumed to be due to the conversion of the In_2O_3 surface to In_2S_3 , which prevents the preferential growth of In_2O_3 and favors a structured growth mode.

This explanation also agrees with observations of Weng *et al.* [Weng '92], who investigated the selenization of 0.5 μm thick pc- In_2O_3 thin films in selenium vapor at temperatures between 400 °C and 500 °C. These authors also concluded that the selenization initially took place as a surface reaction, and proceeded by diffusion afterwards.

In order to verify the proposed mechanism for the sulfurization of In_2O_3 during the H_2S step of the Spray ILGAR deposition process for $\text{In}_2(\text{O,S})_3$ thin films, a more detailed study of the growth process would be needed (e.g. by in-situ XRD or Raman spectroscopy). However, in the growth process of Spray ILGAR CuInS_2 thin films, which are in the focus of this thesis, this growth mechanism is altered by the consumption of In_2S_3 due to CuInS_2 -formation, which is discussed in the following.

Initial CuInS₂ formation

At the deposition temperature of 430 °C, In_2S_3 and Cu_{2-x}S can form CuInS_2 , wherever they are in contact with each other, as it can be seen from the phase diagram in Fig. 2.4 [Binsma '80; Krunks '97]. This means that in the growth of Spray ILGAR CuInS_2 thin films, In_2S_3 can be consumed by the formation of CuInS_2 , if Cu_{2-x}S grains exist near the $\text{In}_2\text{O}_3/\text{In}_2\text{S}_3$ grain. Thus, the sulfurization of In_2O_3 should be able to proceed further than in the case of the Spray ILGAR $\text{In}_2(\text{O,S})_3$ thin films, since In_2S_3 can be removed from the reaction sites by diffusing into the newly formed CuInS_2 grains.

Microscopically, the formation of CuInS_2 from In_2S_3 and Cu_{2-x}S is likely to proceed via the diffusion of indium into the grains of Cu_{2-x}S . For the system Cu-In-S, this process has not been reported in the literature. The structurally and chemically similar system Cu-In-Se has. The diffusion of indium into Cu_2Se was investigated by Park *et al.* in a $\text{Cu}_2\text{Se}/\text{In}_2\text{Se}_3$ diffusion couple [Park '00]. These authors observed the diffusion of indium into Cu_2Se , which led to the precipitation of CuInSe_2 inside the Cu_2Se volume of the couple. They proposed the diffusion of indium to proceed via copper vacancies (V_{Cu}) in Cu_2Se and determined a self-diffusion coefficient of $D_{\text{Cu}_2\text{Se}}^{\text{In}} \approx 4.2 \cdot 10^{-6} \text{ cm}^2 \text{ s}^{-1}$ (at 650 °C). If this value is assumed also to be valid for the diffusion of indium in Cu_{2-x}S , the diffusion length within the duration of the H_2S step of 20 s follows as $L_{D_{\text{Cu}_2\text{S}}^{\text{In}}} = \sqrt{D_{\text{Cu}_2\text{S}}^{\text{In}} \cdot \Delta t_{\text{H}_2\text{S}}} \approx 90 \mu\text{m}$. This is three orders of magnitude greater than the average grain diameter (100 nm) of the copper- and In_2O_3 -containing precursor layer (Fig. 4.7), which is deposited in the spray step of the Spray ILGAR CuInS_2 deposition process. Thus, it may be assumed that even at a deposition temperature of 430 °C, the diffusion length of indium in Cu_{2-x}S is still sufficiently high, so that all In_2S_3 is consumed by the formation of CuInS_2 , provided it is in contact with Cu_{2-x}S grains. Therefore, the amount of CuInS_2 that is formed during the H_2S step of the ILGAR-cycle can be expected to be limited by the

sulfurization rate of In_2O_3 (see above). This also explains why no indication for the presence of In_2S_3 was found by XRD in the characterization of the Spray ILGAR CuInS_2 thin films in section 3.3.2. Due to the low coverage of the substrate after the first spray step of CuInS_2 Spray ILGAR deposition process (Fig. 4.7), it may be that after the first ILGAR-cycle, some $\text{In}_2\text{O}_3/\text{In}_2\text{S}_3$ grains are not in contact with Cu_{2-x}S grains, so that indium cannot diffuse into these grains to form CuInS_2 . Thus, after the first cycle, some In_2S_3 may remain in the layer. However, this In_2S_3 will be consumed in the subsequent cycles, as soon as the substrate is covered completely by $\text{In}_2\text{O}_3/\text{In}_2\text{S}_3$, Cu_{2-x}S and CuInS_2 grains (after 2-3 ILGAR-cycles). The deposition process of copper and In_2O_3 in the first spray step and the subsequent sulfurization and CuInS_2 formation during the H_2S step of the Spray ILGAR process are schematically sketched in Fig. 4.11a-c:

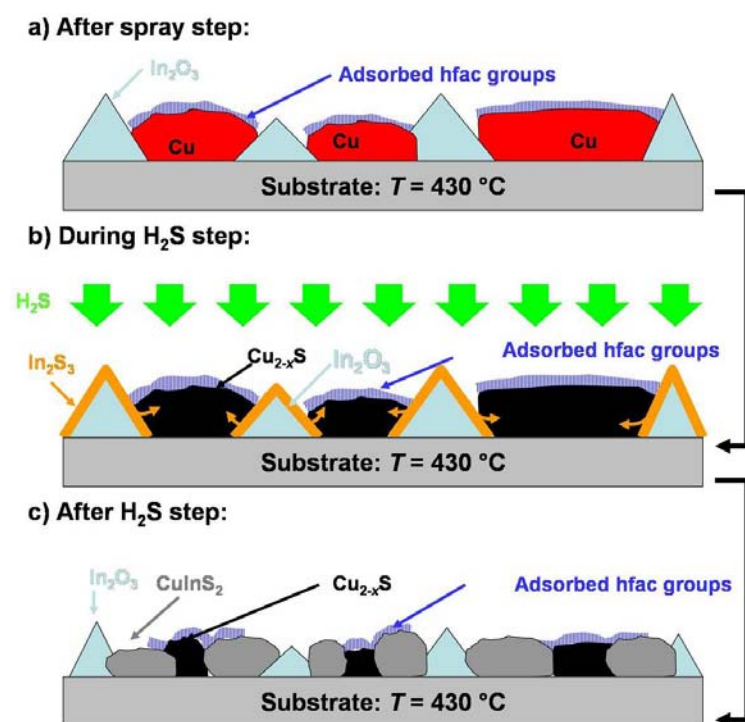


Fig. 4.11: Sketch of the growth processes in the first cycle of the CuInS_2 Spray ILGAR process: After the spray step, the deposited film consists of grains of In_2O_3 and copper (a). The latter may be covered by adsorbed hfac groups (section 4.2.1.). In the H_2S step, the copper grains are completely converted to Cu_{2-x}S , whereas only the surface of the In_2O_3 grains is sulfurized to In_2S_3 (b). This In_2S_3 reacts with Cu_{2-x}S to form CuInS_2 (b to c) by the diffusion of indium into the Cu_{2-x}S grains. Afterwards, the In_2O_3 grains are not covered by In_2S_3 anymore (c).

During the spray step, copper and In_2O_3 grains are deposited, as described in sections 4.2.1. and 4.2.2., respectively. Thus, at the end of the spray step (Fig. 4.11a), the deposited film consists of copper and In_2O_3 grains. Thereby the copper grains may be partially covered by adsorbed hfac groups¹². In the subsequent H_2S step (Fig. 4.11b), the copper grains are completely converted to Cu_{2-x}S , whereas only a surface layer of the In_2O_3 grains is sulfurized to In_2S_3 . This In_2S_3 is then completely consumed by the reaction with Cu_{2-x}S , which yields CuInS_2 , so that the In_2O_3 grains are not covered by In_2S_3 anymore (Fig. 4.11c). Subsequently, the deposition process can proceed by a new spray step, i.e. a new ILGAR-cycle.

4.4. Composition and Morphology of Spray ILGAR CuInS_2 Thin Films

So far, only the deposition and sulfurization processes that occur during the first ILGAR-cycle have been discussed. Since the Spray ILGAR process is a cyclic process, it can be assumed that the processes that occur during the single cycles of the process are equivalent. However,

¹² The presence of these groups does not hinder the sulfurization process for spray step durations of about 30 s because at this point the hfac groups can be expected not to cover the grains completely (page 60). Since the sulfurization of copper proceeds by the fast diffusion of copper out of the grain (page 63), already small free surface areas enable the complete sulfurization of the grain within the duration of the H_2S step.

it is likely that diffusion processes of some elements occur between grains, which were deposited in different cycles. In order to investigate such processes and their influence on the properties of the Spray ILGAR CuInS_2 thin films, the composition (section 4.4.1.) and morphology (section 4.4.2.) of Spray ILGAR CuInS_2 films is investigated in the following.

4.4.1. Compositional Analysis of Spray ILGAR CuInS_2 Thin Films

In this section, the composition of Spray ILGAR CuInS_2 thin films (section 3.3.2.) is investigated as a basis for the deduction of a model for the growth of Spray ILGAR CuInS_2 thin films. In particular, the amount of In_2O_3 that is present in the as-deposited films, i.e. prior to the post-deposition H_2S annealing, is estimated in order to reveal its dependence on the choice of the preparation parameters (spray and H_2S step duration and $[\text{Cu}]:[\text{In}]$ ratio of the spraying solution).

In section 3.3.2., it was shown that Spray ILGAR CuInS_2 thin films could be prepared by using the preparation parameters in Table 3.6. In order to investigate the influence of these parameters on the film composition and in particular on the In_2O_3 content, nine CuInS_2 thin films were studied (Samples 329, 330, 412-418). The preparation parameters of these films are listed in Table 4.2. All other parameters were identical to those listed in Table 3.6. The $[\text{Cu}]:[\text{In}]$ ratio of the spraying solution was varied between 1.0 and 2.0. No copper-poor solutions were investigated, in order to avoid the formation of CuIn_5S_8 (Fig. 2.4). The duration of the H_2S step in the ILGAR-cycle was chosen between 20 s and 120 s in order to vary the amount of In_2O_3 in the as-deposited films. No H_2S step durations longer than 120 s were investigated, in order to keep the deposition rate of the process in a reasonable range (≥ 10 nm/min; page 25).

Table 4.2: Preparation parameters of Spray ILGAR CuInS_2 thin films, which were prepared using the process described in section 3.3.2: $[\text{Cu}]:[\text{In}]$ ratio of the spraying solution, duration of the spray- and H_2S steps of the ILGAR-cycle, amount of $\text{Cu}(\text{hfac})_2$ and InCl_3 solution (both 40 mM) in the spraying solution and number of ILGAR-cycles. All other preparation parameters were identical to those listed in Table 3.6. Refer to Appendix I for a complete list of the preparation parameters.

Sample	329	330	412	413	414	415	416	417	418
$[\text{Cu}]:[\text{In}]$ ratio of spraying solution	1	1.25	1.25	1.25	1.5	1.75	2	1.75	1.25
Spray step duration [s]	30	30	30	20	30	30	30	30	30
H_2S step duration [s]	20	20	40	120	20	20	20	40	60
Duration of H_2S annealing [min]	15	15	45	45	15	15	15	15	90
Amount of $\text{Cu}(\text{hfac})_2$ solution [ml]	25	25	12.5	25	25	25	25	25	25
Amount of InCl_3 solution [ml]	25	20	10	20	16.6	14.3	12.5	14.3	20
Number of ILGAR-cycles	24	22	14	23	25	21	23	19	25

The changes in the number of ILGAR-cycles resulted from the variation of the $[\text{Cu}]:[\text{In}]$ ratio of the spraying solutions, since all solutions had a constant molarity of 40 mM (section 3.1.3.). Also the length of the spray step duration influenced the number of ILGAR-cycles, since it determined the amount of solution that was consumed in one cycle.

In order to investigate the influence of the post-deposition H_2S and KCN treatments (sections 3.3.1.-2.), the samples were cut into two halves after deposition. Of these, one remained untreated as it was deposited (“*as-deposited*”) and one was annealed in $\text{Ar}/\text{H}_2\text{S}$ and etched in KCN (“ *H_2S and KCN treated*”). The post-deposition treatments were meant to sulfurize residual In_2O_3 (H_2S) and to remove segregated Cu_{2-x}S (KCN). It was found that the duration of this H_2S annealing influenced the morphology, yet did not effect the composition of the H_2S and KCN treated films for durations longer than 15 min, as they were used in the course of this thesis. The influence of the annealing on the film morphology is discussed in section 4.4.2.5. Hence, in the present section, only a general discussion of the influence of the post-deposition H_2S annealing, independent of duration, is given.

The relative amounts of copper, indium and sulfur in these thin films were measured by XRF and are listed in Table 4.3. for the as-deposited and for the H₂S and KCN treated films. The XRF measurements are described in Appendix VII.iii.

Table 4.3: Relative contents of copper x_{Cu} , indium x_{In} and sulfur x_S , as measured by XRF (Appendix VII.iii), of as-deposited and H₂S and KCN treated Spray ILGAR CuInS₂ thin films that were prepared using the parameters in Table 4.2. The uncertainties are ± 1 at. % for the elemental contents and ± 15 % (relative) for the thickness and deposition rate.

Sample	329	330	412	413	414	415	416	417	418
As-deposited									
Copper content x_{Cu} [mol]	31	31	30	28	32	34	35	34	30
Indium content x_{In} [mol]	29	28	31	27	26	22	22	23	26
Sulfur content x_S [mol]	40	41	39	45	43	44	43	43	44
H₂S and KCN treated									
Copper content x_{Cu} [mol]	24	24	25	23	24	24	24	24	24
Indium content x_{In} [mol]	27	26	26	24	26	26	26	26	26
Sulfur content x_S [mol]	49	50	50	52	50	50	50	49	50
Thickness [nm]	1034	743	447	603	664	538	508	506	792
Deposition rate [nm/min]	37	29	21	10	23	22	19	18	17

The data shows that compared to stoichiometric CuInS₂ all as-deposited films are sulfur-poor. This indicates the presence of In₂O₃, due to its incomplete sulfurization in the H₂S step. This was also confirmed by XRD measurements, which detected In₂O₃ in all of the as-deposited films in Table 4.4. (Fig. 3.11a for samples 329 and 330). Based on the results of sections 4.2. and 4.3., it may be assumed that depending on the [Cu]:[In] ratio of the precursor solution, the as-deposited films also contain Cu_{2-x}S as a secondary phase. In contrast, independently of the annealing conditions, the composition of all H₂S and KCN treated films agrees with the stoichiometry of a KCN etched RTP-CuInS₂ reference thin film (24 ± 1 % copper, 26 ± 1 % indium, 50 ± 1 % sulfur), which was determined by ERDA.

In order to evaluate the data in Table 4.3. with respect to the influence of the deposition parameters on the composition of the Spray ILGAR CuInS₂ thin films, the amount of In₂O₃ in the as-deposited films needs to be determined. Therefore, it would be desirable to measure the oxygen content of the films. Since light elements, such as oxygen cannot be measured precisely by XRF (Appendix VII.iii), the In₂O₃ content of the films was estimated from the XRF data in Table 4.3. In the following, this estimation procedure is explained. Firstly, it was assumed that no phases other than CuInS₂, In₂O₃ and Cu₂S exist in the films, which contain copper, indium or sulfur. Thereby, for the sake of simplicity, all copper sulfide was assumed to be present as Cu₂S. If x_{Cu} , x_{In} and x_S are the relative molar contents of copper, indium and sulfur in a certain film (measured by XRF; Table 4.3) and y_{Cu_2S} , $y_{In_2O_3}$ and y_{CuInS_2} are the relative molar amounts of Cu₂S, In₂O₃ and CuInS₂, the following equations are valid:

$$2 \cdot y_{Cu_2S} + y_{CuInS_2} = x_{Cu} \quad \text{Eq. (4.23a)}$$

$$\text{and} \quad y_{Cu_2S} + 2 \cdot y_{CuInS_2} = x_S \quad \text{Eq. (4.23b)}$$

From Eq. (4.23a, b), equations for y_{CuInS_2} and y_{Cu_2S} can be deduced, which only depend on x_{Cu} and x_S :

$$y_{CuInS_2} = (2 \cdot x_S - x_{Cu}) / 3 \quad \text{Eq. (4.23c)}$$

$$\text{and} \quad y_{Cu_2S} = (2 \cdot x_{Cu} - x_S) / 3 \quad \text{Eq. (4.23d)}$$

After calculating the relative molar contents of CuInS₂ and Cu₂S according to Eq. (4.23c, d), the amount of In₂O₃ $y_{In_2O_3}$ follows from the residual indium-excess:

$$y_{In_2O_3} = (x_{In} - y_{CuInS_2}) / 2 \quad \text{Eq. (4.23e)}$$

According to Eq. (4.23a-e), values for $y_{\text{Cu}_2\text{S}}$, $y_{\text{In}_2\text{O}_3}$ and y_{CuInS_2} for the Spray ILGAR CuInS_2 thin films in Table 4.4 were calculated. In order to obtain the relative molar amounts from these values, their sum was set to 100 %. The relative molar amount X_{Compound} of the respective compound Cu_2S , In_2O_3 or CuInS_2 was then calculated as:

$$X_{\text{Compound}} = \frac{y_{\text{Compound}}}{y_{\text{Cu}_2\text{S}} + y_{\text{In}_2\text{O}_3} + y_{\text{CuInS}_2}} \quad \text{Eq. (4.23f)}$$

The calculated values for the relative molar amounts of Cu_2S , In_2O_3 and CuInS_2 , as obtained from the XRF data in Table 4.3, are listed in Table 4.4. The uncertainties of these values are mainly due to the presence of Cu_{2-x}S ($0 \leq x \leq 0.2$) phases with $[\text{Cu}]:[\text{S}]$ ratios below two and to a slightly indium-rich (about 1 at. %) composition of CuInS_2 after KCN etching. From these values and Eq. (4.23a-f), the uncertainties of the relative molar amounts of Cu_2S , In_2O_3 and CuInS_2 were determined as, and $\Delta X_{\text{Cu}_2\text{S}} = \pm 6$ mol. %, $\Delta X_{\text{In}_2\text{O}_3} = \pm 2$ mol. %, and $\Delta X_{\text{CuInS}_2} = \pm 3$ mol. %.

Table 4.4: Relative molar amounts of Cu_2S $y_{\text{Cu}_2\text{S}}$, In_2O_3 $y_{\text{In}_2\text{O}_3}$ and CuInS_2 y_{CuInS_2} (mol. %) as estimated from the XRF-measured relative amounts of copper, indium and sulfur for as-deposited and H_2S and KCN treated Spray ILGAR CuInS_2 films (Tables 4.2 and 4.3). Eq. (4.23a-f) were used for the estimation. The uncertainties of the relative molar amounts of Cu_2S , In_2O_3 and CuInS_2 (mol. %) were determined to as $\Delta X_{\text{Cu}_2\text{S}} = \pm 6$ mol. %, $\Delta X_{\text{In}_2\text{O}_3} = \pm 2$ mol. %, and $\Delta X_{\text{CuInS}_2} = \pm 3$ mol. %.

Sample	329	330	412	413	414	415	416	417	418
As-deposited									
Cu_2S $y_{\text{Cu}_2\text{S}}$ [mol. %]	24	24	23	13	24	29	32	30	18
In_2O_3 $y_{\text{In}_2\text{O}_3}$ [mol. %]	21	19	25	12	14	7	9	8	12
CuInS_2 y_{CuInS_2} [mol. %]	54	58	52	75	62	64	60	62	71
H_2S and KCN treated									
Cu_2S $y_{\text{Cu}_2\text{S}}$ [mol. %]	0	0	0	0	0	0	0	0	0
In_2O_3 $y_{\text{In}_2\text{O}_3}$ [mol. %]	5	1	2	0	2	2	2	3	1
CuInS_2 y_{CuInS_2} [mol. %]	95	99	98	100	99	99	99	97	99

The estimated compositions of the as-deposited (gray symbols) and H_2S and KCN treated Spray-ILGAR CuInS_2 (black symbols) thin films are visualized in a ternary composition diagram in Fig. 4.12 according to the values in Table 4.4.

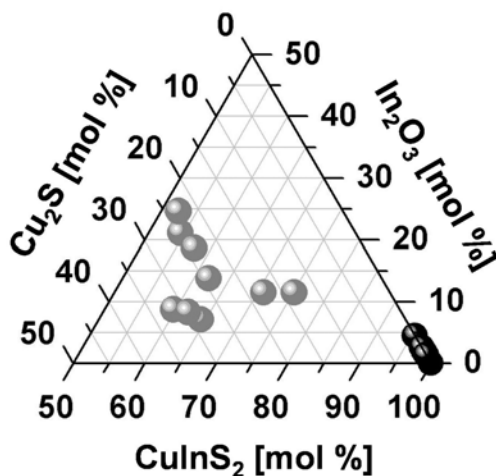


Fig. 4.12: Ternary composition diagram of the as-deposited (gray symbols) and H_2S and KCN treated Spray ILGAR CuInS_2 (black symbols) thin films. The relative molar contents of Cu_2S $y_{\text{Cu}_2\text{S}}$, In_2O_3 $y_{\text{In}_2\text{O}_3}$ and CuInS_2 y_{CuInS_2} (Table 4.4) have been estimated from the XRF-results in Table 4.3. according to Eq. (4.23a-f). See Appendix I for a list of all preparation parameters of these films.

After the post-deposition H_2S and KCN treatments, the estimated compositions of the investigated Spray ILGAR CuInS_2 thin films agree, within their uncertainties, with that of a stoichiometric CuInS_2 thin film, independently of the precise annealing conditions. This is consistent with XRD measurements, which detected no other phase than CuInS_2 in these films

(Fig. 3.11b for samples 329 and 330). Thus, already after a post-deposition H_2S annealing of 15 min at $550\text{ }^\circ\text{C}$, all In_2O_3 , which was present in the as-deposited films, has been sulfurized completely¹³.

In contrast to the H_2S and KCN etched Spray ILGAR CuInS_2 thin films, the as-deposited films contain between $13\text{-}32 \pm 6$ mol. % Cu_2S and $7\text{-}25 \pm 2$ mol. % In_2O_3 . Based on these estimated Cu_2S -, In_2O_3 - and CuInS_2 contents, the influence of the preparation parameters (Table 4.2) on the composition of the as-deposited films can be discussed. The comparison of the preparation conditions with the film compositions in Table 4.4 reveals that the amount of Cu_2S , In_2O_3 and CuInS_2 in the as-deposited Spray ILGAR CuInS_2 films is mainly determined by the duration of the spray step $\Delta t_{\text{Spray step}}$ and the H_2S step $\Delta t_{\text{H}_2\text{S step}}$ of the ILGAR-cycle, as well as by the $[\text{Cu}]:[\text{In}]$ ratio of the spraying solutions. The influence of these parameters on the composition of the as-deposited Spray ILGAR CuInS_2 thin films is discussed in the following.

In Fig. 4.13a, the relative molar contents of Cu_2S , CuInS_2 , In_2O_3 from Table 4.4 are plotted as a function of the ratio of the duration of the spray step $\Delta t_{\text{Spray step}}$ and the H_2S step $\Delta t_{\text{H}_2\text{S step}}$ of the ILGAR-cycle for as-deposited Spray ILGAR CuInS_2 thin films, which were all deposited from spraying solutions of a $[\text{Cu}]:[\text{In}]$ ratio of 1.25 (samples 330, 412, 413 and 418). In Fig. 4.13b, the influence of the $[\text{Cu}]:[\text{In}]$ ratio of the spraying solution of the film composition is depicted (samples 329, 330, 414-416) for films deposited with spray- and H_2S step durations of 30 s and 20 s, respectively.

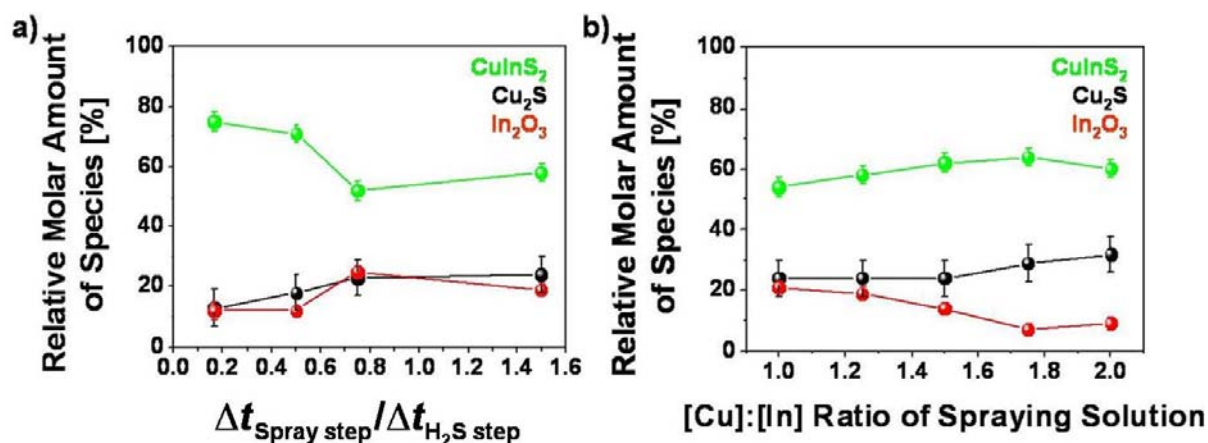


Fig. 4.13: Influence of the preparation parameters on the composition of as-deposited Spray ILGAR CuInS_2 thin films: a) Influence of the ratio of the durations of the spray- and H_2S steps of the ILGAR-cycle. b) Influence of the $[\text{Cu}]:[\text{In}]$ ratio of the spraying solution. The preparation parameters for these films (samples 330, 412, 413 and 418) are listed in Table 4.2. The relative molar amounts of CuInS_2 , Cu_2S and In_2O_3 have been estimated from XRF-results (Table 4.3) according to Eq. (4.23a-f) and are listed in Table 4.4.

For small ratios of the spray- and H_2S step durations of the ILGAR-cycle, the CuInS_2 content increases, whilst the Cu_2S - and In_2O_3 contents decrease (Fig. 4.13a). The duration of the spray step determines the amount of precursor material (copper and In_2O_3) that is deposited in the ILGAR-cycle, whereas the H_2S step duration limits the time, in which this amount of precursor material can be sulfurized. Fig. 4.13a indicates that the growth of CuInS_2 is limited by the incomplete sulfurization of In_2O_3 and the subsequent diffusion of indium into the Cu_2S

¹³ The apparent non-zero In_2O_3 content of the H_2S and KCN treated films in Table 4.4 and Fig. 4.12 may also result from the slightly indium-rich composition (about 1 at. % compared to stoichiometric CuInS_2) of KCN etched CuInS_2 thin films [Hashimoto '95]. This composition was found to be caused by a copper-depletion of the surface of KCN etched CuInS_2 thin films [Hashimoto '95]. Since Eq. (4.23a-f) assumed a stoichiometric CuInS_2 composition, an indium-rich composition will result in a non-zero In_2O_3 content (Eq. (4.23e)).

domains, which leads to the formation of CuInS_2 on the expense of Cu_2S and In_2O_3 , and thus confirms the assumptions made in section 4.3, that the CuInS_2 formation is limited by the incomplete sulfurization of In_2O_3 (Fig. 4.11).

Fig. 4.13b shows that the contents of CuInS_2 and Cu_2S increase with an increasing $[\text{Cu}]:[\text{In}]$ ratio of the spraying solution up to a $[\text{Cu}]:[\text{In}]$ ratio of 1.75, whereas the In_2O_3 content decreases. This was expected, since the composition of the deposited film reflects the $[\text{Cu}]:[\text{In}]$ ratio of the spraying solution. At a $[\text{Cu}]:[\text{In}]$ ratio of two, a slightly decreased CuInS_2 content was found, while the Cu_2S - and In_2O_3 contents were slightly increased compared to the values at a $[\text{Cu}]:[\text{In}]$ ratio of 1.75. The differences are, however, smaller than the error of the data and thus their physical relevance is questionable. It may also be that the large copper-excess led to the partial inclusion of the In_2O_3 domains and thus hindered the sulfurization of In_2O_3 and the formation of CuInS_2 .

In conclusion, the composition data in Fig. 4.13a and b reveal that the formation of In_2O_3 cannot be avoided by an appropriate choice of the deposition parameters, since even for spray- and H_2S step durations of 20 s and 120 s (sample 413; $\Delta t_{\text{Spray step}}/\Delta t_{\text{H}_2\text{S step}} = 0.17$), the In_2O_3 content of the film still was 12 ± 2 mol. %. Also for a $[\text{Cu}]:[\text{In}]$ ratio as high as 1.75 (sample 415), an In_2O_3 content of 7 ± 2 mol. % was found. According to Fig. 4.13b, a further increase of the $[\text{Cu}]:[\text{In}]$ ratio cannot be expected to result in a further decrease of the In_2O_3 content. A further decrease of the $\Delta t_{\text{Spray step}}/\Delta t_{\text{H}_2\text{S step}}$ ratio has to be excluded for practical reasons because it would lead to longer durations of the ILGAR-cycle and thus further reduce the deposition rate in the experiments. The deposition rate of sample 413 of 10 ± 2 nm/min (Table 4.3) was already lower than the desired rate of 20-30 nm/min (section 2.3., p.18). This means that the approach of sulfurizing In_2O_3 in a post-deposition H_2S annealing, made in section 3.3.2., is most promising in order to obtain single-phase CuInS_2 thin films.

4.4.2. Correlation of Composition and Morphology

The layered morphology of the Spray ILGAR CuInS_2 thin films (Fig. 3.13) is analyzed in this section by correlating the film morphology to the phases present in the film. Due to the different diffusion processes that occur in these phases (section 4.3.), their distribution in the film, which is revealed in this section, determines the diffusion paths and thus the growth behavior of the films. In sections 4.4.2.1.-3., the distribution of Cu_{2-x}S and In_2O_3 in the films is studied, whereas in sections 4.4.2.4. and 4.4.2.5., the composition and morphology of the *layered bottom layer* and the *well-crystallized top layer* of the H_2S and KCN treated films is investigated (Fig. 3.13b, d).

Together with the analysis of the deposition and sulfurization processes of the copper- and In_2O_3 -containing precursor layer (sections 4.2. and 4.3.), the results of this section allow for the formulation of a model for the overall growth process of Spray ILGAR CuInS_2 thin films, which is proposed in section 4.5.

For the investigations of sections 4.4.2.1.-3., the same samples are used, whose compositions were determined in section 4.4.1. (samples 329, 330, 412-418; Table 4.4). It was, however, found by SEM that the morphology of all of these films qualitatively agreed with that observed in Fig. 3.13a and c, independently of the preparation parameters. Therefore, the results obtained in sections 4.4.2.1.-3., can be expected to be representative for all Spray ILGAR CuInS_2 thin films.

For sections 4.4.2.4. and 4.4.2.5., new samples were prepared based on the findings of section 4.4.1., in order to investigate the influence of the film composition and of the post-deposition H_2S annealing on the properties of the *layered bottom layer* and the *well-crystallized top layer* of the Spray ILGAR CuInS_2 thin films.

4.4.2.1. Distribution of Cu_{2-x}S in As-Deposited Spray ILGAR CuInS_2 Thin Films

In order to reveal the location of Cu_{2-x}S in the as-deposited Spray ILGAR CuInS_2 thin films, the cross-section of such a film (sample 412; Table 4.2) was investigated by SEM (Fig. 4.14a). Additionally, the same film was etched in KCN and the cross-section was again characterized by SEM (Fig. 4.14b). The KCN etching is meant to selectively remove segregated Cu_{2-x}S from the film surface [Weber '02], since from the three phases, which are present in the film (Cu_{2-x}S , CuInS_2 , In_2O_3), only Cu_{2-x}S is sensitive to KCN etching [Sandmann '00; Weber '02]. In chalcopyrite thin films, binary copper-chalcogen-phases are commonly observed to segregate on the film surface [Klenk '93; Scheer '94; Scheer '95].

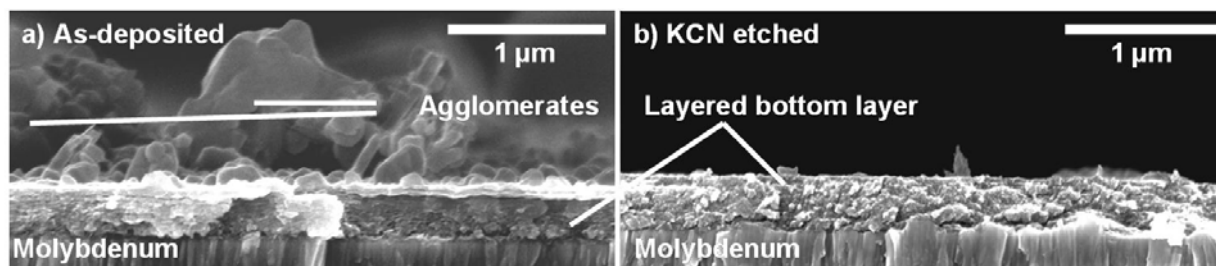


Fig. 4.14: a) Cross-sectional SEM image of an as-deposited Spray ILGAR CuInS_2 thin film (sample 412). b) Cross-sectional SEM image of the same film after KCN etching. The preparation parameters of the film are listed in Table 4.2.

It can be seen from Fig. 4.14 that the KCN etching changes the film morphology. The as-deposited film consists of a nanocrystalline *layered bottom layer*, on which agglomerates of a diameter of up to $1\ \mu\text{m}$ are observed (Fig. 4.14a). After KCN etching, the agglomerates are removed whilst the *layered bottom layer* remains without any observable changes (Fig. 4.14b). This suggests that the agglomerates consist of Cu_{2-x}S , whereas the *layered bottom layer* may consist of CuInS_2 and In_2O_3 , which are insensitive to KCN [Sandmann '00; Weber '02].

Even though Cu_{2-x}S is present in all as-deposited Spray ILGAR CuInS_2 thin films (Table 4.4), it was not detected in any X-ray diffractograms in the course of this thesis (Fig. 3.11a). This indicates that it is present in an amorphous or nanocrystalline state and is thus not observable by XRD. This agrees with the morphology of the Cu_{2-x}S agglomerates in Fig. 4.14a, where no crystalline facets are visible.

4.4.2.2. Distribution of In_2O_3 in As-Deposited Spray ILGAR CuInS_2 Thin Films

In this section, the distribution of In_2O_3 in the as-deposited Spray ILGAR CuInS_2 thin films is analyzed. In the previous section, it was shown that the agglomerates on the surface of the as-deposited Spray ILGAR CuInS_2 films consist of Cu_{2-x}S . Consequently, In_2O_3 and CuInS_2 must be located in the *layered bottom layer*. In order to study the distributions of In_2O_3 and CuInS_2 in the *layered bottom layer*, an as-deposited Spray ILGAR CuInS_2 thin film (sample 330) was etched in KCN (Cu_{2-x}S removal) and characterized by SEM and EDX.

Fig. 4.15a-e show the SEM image and the EDX elemental intensity maps of the O-K, S-K, In-L, and Cu-L X-ray lines. The brightness within the maps represents the intensity of the EDX signal of the corresponding elements: White indicates high and black low intensity.

The SEM image (Fig. 4.15a) reveals that the sample surface is inhomogeneous, as it was also observed for the as-deposited film in section 3.3.2 (Fig. 3.12g-i). Besides large agglomerates with diameters of several micrometers, which are scarcely distributed on the surface, two areas of different morphology can be distinguished: A inhomogeneously structured region is found in the center of the image (upper left to lower right corner; Fig. 4.15a), whereas the rest of the surface appears homogeneous without any observable structure (lower left and upper

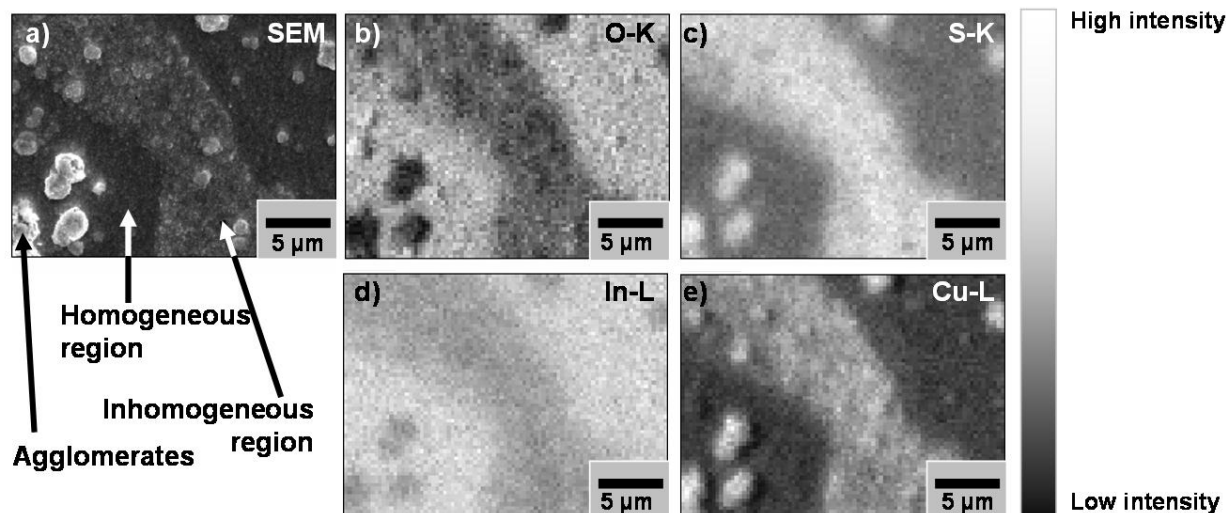


Fig. 4.15: a) Plan - view SEM image of a KCN etched as-deposited Spray ILGAR CuInS_2 thin film (sample 330) and EDX elemental intensity maps of the O-K (b), S-K (c), In-L (d), and Cu-L (e) X-ray lines. See Table 4.2 for preparation parameters

right corner; Fig. 4.15a). These morphological differences are correlated to the distribution of the elements: Copper and sulfur are mainly found in the inhomogeneous parts and in the agglomerates (Fig. 4.15c, e), whereas oxygen is only found in the homogeneous part (Fig. 4.15b). Indium is detected in all parts, but is slightly higher concentrated in the homogeneous part (Fig. 4.15d). This suggests that the homogeneous part contains a large amount of In_2O_3 ¹⁴, whereas the inhomogeneous regions and the agglomerates seem to consist mainly of CuInS_2 . The origin of the different morphologies remains unclear at this point and will be analyzed in the following.

4.4.2.3. Surface Composition of Spray ILGAR CuInS_2 Thin Films

This section focuses on the identification of the phases, which are present at the surface of as-deposited as well as of the H_2S and KCN treated Spray ILGAR CuInS_2 thin films. The comparison of these measurements with each other and with the bulk composition that was revealed in sections 4.4.2.1. and 4.4.2.2., may shed some light on the diffusion processes that occur during the growth of these films and thus help to deduce a growth model.

XPS and Auger spectroscopy were chosen for these investigations, since they only probe the upmost monolayers of the films and are sensitive to changes in the chemical bonds of the elements (Appendix VII.i). In order to identify the phases present at the surface of the Spray ILGAR CuInS_2 thin films, a Spray ILGAR Cu_{2-x}S thin film, a sprayed In_2O_3 thin film and a KCN etched RTP- CuInS_2 thin film served as references for the respective compounds.

The $\text{CuL}_3\text{M}_{45}\text{M}_{45}$ Auger- and $\text{In}3d$ XPS spectra of an as-deposited and of a H_2S and KCN treated Spray ILGAR CuInS_2 thin film are compared to the reference spectra in Fig. 4.16.

The spectra obtained from the as-deposited Spray ILGAR CuInS_2 thin film (sample 412) agree well with those of the Cu_{2-x}S and In_2O_3 references, which indicates that the surface of this film consists only of Cu_{2-x}S and In_2O_3 . This means that all CuInS_2 is covered completely by Cu_{2-x}S , whereas In_2O_3 is not covered. This is strong evidence that the diffusion of Cu_{2-x}S to the film surface took place through the CuInS_2 regions of the film. However, the coverage of CuInS_2 with Cu_{2-x}S may be less pronounced for films containing less Cu_{2-x}S .

¹⁴ Raman spectroscopy revealed that CuInS_2 is also present in these regions, but presumably not in the surface-near regions of the film (see section 5.2.).

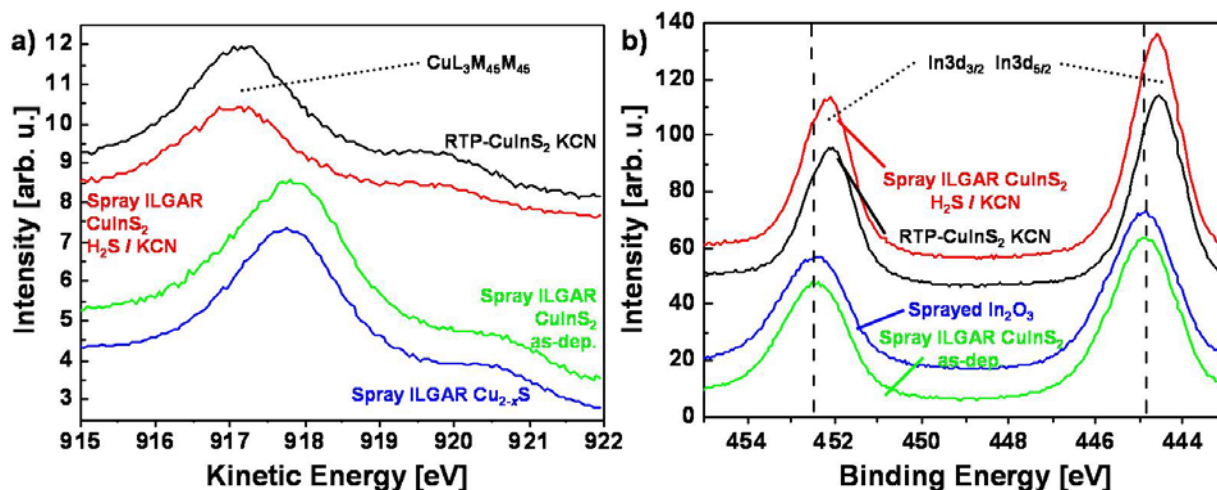


Fig. 4.16: Comparison of Auger- and XPS spectra of as-deposited and H₂S and KCN treated Spray ILGAR CuInS₂ thin films (sample 412) with the CuL₃M₄₅M₄₅ spectra of a RTP-CuInS₂ and a Spray ILGAR Cu_{2-x}S thin film (a) and with the In3d_{5/2} and In3d_{3/2} spectra of a RTP-CuInS₂ and an In₂O₃ thin film (b). The Cu_{2-x}S and In₂O₃ thin films were prepared as described in sections 3.1.3. and 4.2.2. The preparation parameters of all samples are listed in Appendix I. An ALK α X-ray source was used for excitation (1486.6 eV). The spectra are shifted for the sake of clarity.

The CuL₃M₄₅M₄₅ and In3d spectra of the H₂S and KCN treated Spray ILGAR CuInS₂ thin films coincide with those of the RTP-CuInS₂ reference film. The same was true for all other copper, indium and sulfur signals of the films. These results agree well with the results of the bulk-analysis of the Spray ILGAR CuInS₂ thin films in sections 3.3.2. and 4.4.1., which detected no other phase than CuInS₂ in the H₂S and KCN treated Spray ILGAR CuInS₂ thin films. In particular, this means that the *well-crystallized top layer* of these films (Fig. 3.13b, d), which is formed during the post-deposition H₂S annealing, consists of CuInS₂.

4.4.2.4. Carbon in the Layered Bottom Layer of Spray ILGAR CuInS₂ Thin Films

In order to formulate a model for the growth of Spray ILGAR CuInS₂ thin films, the layered morphology that is observed in the *layered bottom layer* (Fig. 3.13) of the films, must be understood. In this section the origin of this layered morphology is analyzed by TEM and EDX measurements.

As mentioned in section 3.3.2., the number of layers in the *layered bottom layer* corresponds to the number of ILGAR-cycles during the deposition process of the films. It was also found that the number and the appearance (as observed by SEM) of these layers did not change upon H₂S annealing. In order to reveal the origin of these layers, the cross-section of an H₂S annealed Spray ILGAR CuInS₂ thin film (sample 419; Appendix I) was characterized by TEM and EDX (Appendix VII.iv). In Fig. 4.17, the results of these investigations are shown. Fig. 4.17a shows a cross-sectional TEM image of the *layered bottom layer* of the film. The layers consist of uniform grains and are separated by nanocrystalline or amorphous interlayers. An EDX line-scan across these layers (Fig. 4.17b) showed that the interlayers are poor in copper, indium and sulfur. Elemental distribution maps of sulfur and carbon of this region, obtained by energy-filtered TEM (Fig. 4.17c, d), proved that low sulfur-concentration coincides with high carbon-concentration and vice versa. Thus, the CuInS₂ layers are separated by carbon-rich layers¹⁵.

¹⁵ In section 5.3., the carbon-containing compound in the interlayers is characterized by Raman spectroscopy. Raman spectroscopy showed that the presence of these carbon-containing interlayers is inherent to the Spray ILGAR CuInS₂ thin films and no artifact of e.g. the TEM sample preparation.

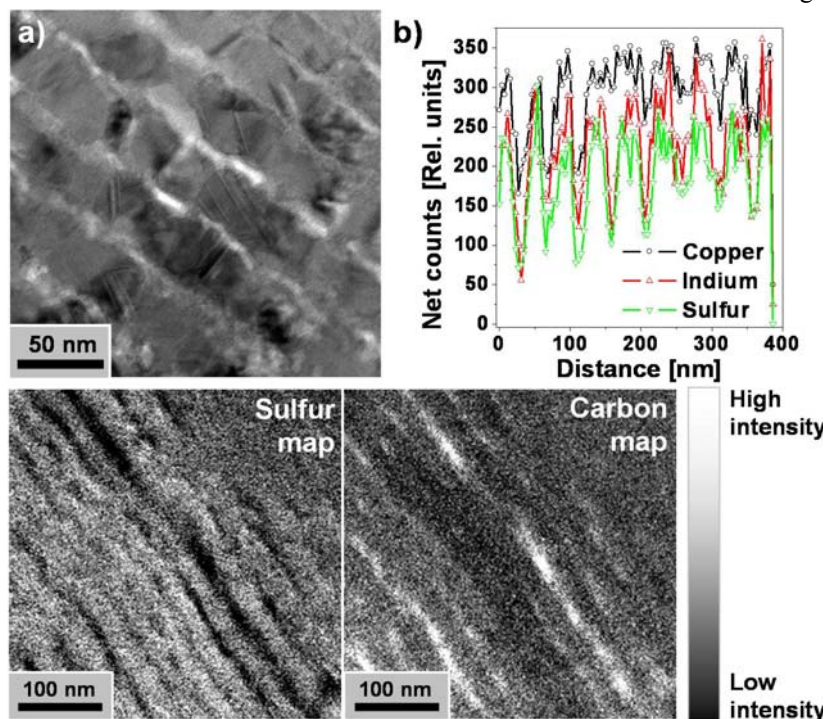


Fig. 4.17: TEM-analysis of the cross-section the *layered bottom layer* of a H_2S annealed Spray ILGAR CuInS_2 thin film (sample 419): a) TEM bright-field image; b) EDX linescan across the layers. c-d) Energy-filtered TEM elemental distribution maps of sulfur (c) and carbon (d). The preparation parameters are listed in Appendix I. The TEM measurements are described in Appendix VII.iv.

The amount of carbon was quantified by ERDA for an as-deposited and for a H_2S and KCN treated Spray ILGAR CuInS_2 thin film (sample 413; Appendix I). These measurements revealed a carbon content of 5 ± 1 at. % for both films. Based on the mechanism for the deposition of copper in the spray step of the ILGAR-cycle that was proposed in section 4.2.1. and 4.2.3., the carbon in these interlayers may be assumed to originate from the hfac groups of the $\text{Cu}(\text{hfac})_2$ compound, which remain adsorbed on the surface of the deposited copper, if too little water is present during the deposition process. This would cause the formation of a carbon-rich layer on top of the deposited precursor layer in every spray step of the ILGAR-cycle. This layer may prevent a homogeneous growth of the material that is deposited in two subsequent ILGAR-cycles and thus cause the layered morphology observed in the *layered bottom layer* of the Spray ILGAR CuInS_2 thin films (Fig. 3.13).

4.4.2.5. Formation of the *Well-Crystallized Top Layer* in Spray ILGAR CuInS_2 Thin Films

The formation of the *well-crystallized top layer* of the Spray ILGAR CuInS_2 thin films (Fig. 3.13d), which forms during the post-deposition H_2S annealing, is analyzed in this section. The dependence of the *top layer* morphology, on the annealing conditions, and on the original composition of the as-deposited film, is discussed.

Prior to the post-deposition H_2S annealing, i.e. in the as-deposited state, the Spray ILGAR CuInS_2 thin films consist of Cu_{2-x}S , In_2O_3 , CuInS_2 (about 95 at. % of the film) and a carbon-containing compound (about 5 at. %) as a contaminant (sections 4.4.1. and 4.4.2.4.). It was found that these phases are not evenly distributed in the as-deposited films. CuInS_2 and In_2O_3 form a *layered bottom layer*, in which the CuInS_2 - and In_2O_3 -containing layers are separated by carbon-containing interlayers (sections 4.4.2.2. and 4.4.2.4.). On top of the CuInS_2 -containing regions of the *layered bottom layer*, Cu_{2-x}S agglomerates are located (sections 4.4.2.1. and 4.4.2.3.). In section 4.3., it was shown that the amount of CuInS_2 in the as-deposited Spray ILGAR CuInS_2 thin films is limited by the amount of In_2O_3 that is sulfurized in the spray step of the ILGAR-cycle. The In_2O_3 content of the films was found to increase for increasing ratios of the durations of the spray step and the H_2S step and for decreasing $[\text{Cu}]:[\text{In}]$ ratios of the spraying solution (Fig. 4.13).

After the post-deposition H₂S annealing, no In₂O₃ was present in the films anymore, independently of the annealing conditions or the composition of the as-deposited film (Fig. 4.12). This compositional change was accompanied by the formation of a *well-crystallized top layer* of CuInS₂ on top of the *layered bottom layer* (Fig. 3.13b, d). These results indicate that the CuInS₂ *top layer* is formed following the sulfurization of In₂O₃ by the diffusion of indium into the Cu_{2-x}S agglomerates on top of the as-deposited films. If this is so, the thickness of the *well-crystallized top layer* should increase for increasing In₂O₃ contents. The annealing conditions can be expected to affect the *top layer* formation process, since they determine the temperature and duration for the diffusion process.

In order to verify these assumptions, the morphology of the *well-crystallized top layer* of three Spray ILGAR CuInS₂ thin films was characterized by SEM and optical microscopy. The films (samples 419-421; Appendix I) were prepared from slightly copper-poor spraying solutions ([Cu]:[In] = 0.95) in order to increase the amount of In₂O₃ in the as-deposited films but still avoid the formation of CuIn₅S₈¹⁶. The influence of a reduction of the H₂S step duration (at constant spray step duration) from 30 to 10 s was investigated, which should further increase the In₂O₃ content. The annealing conditions were also varied, by adding Ar annealing steps at 375 °C (60 min) and 550 °C (60 min) prior to the H₂S annealing at 550 °C (30 min). This was meant to enhance the diffusion of Cu_{2-x}S in the as-deposited films prior to the H₂S annealing. The durations of the annealing steps were chosen empirically, but quantitative considerations in the next section (section 4.5.) indicate that they could be decreased significantly in order to speed up the process. The annealing temperature of 375 °C was chosen in accordance with previous work of Kropp [Kropp '02]. The annealing temperature of 550 °C was the maximum temperature that could be used without deformation of the glass substrates.

In Fig. 4.18, the cross-sectional SEM (a, c, e) and plan-view optical microscope images (b, d, f) of the H₂S annealed Spray ILGAR CuInS₂ films (samples 419-421) are shown.

The SEM images reveal that no significant change in the thickness of the *well-crystallized top layer* occurs upon the addition of the Ar annealing steps (Fig. 4.18a, c). In contrast, the reduction of the H₂S step duration increased the thickness up to about 1 μm (Fig. 4.18c, e). The plan-view images show that the additional Ar annealing prior to the H₂S annealing leads to an increase of the homogeneity of the *well-crystallized top layer*. In the plan-view image in Fig. 4.18b, agglomerations are visible, which are similar to those that appeared on the films that were analyzed in section 3.3.2. (Fig. 3.12a, g). Upon addition of the Ar annealing steps, no such agglomerates are observed anymore and the surface becomes homogeneous (Fig. 4.18d, f).

These results support the above assumption that the *well-crystallized CuInS₂ top layer* is formed by the diffusion of indium into the Cu_{2-x}S agglomerates on the film surface as soon as the In₂O₃ in the *layered bottom layer* is converted to In₂S₃ by H₂S. Therefore, a maximum amount of In₂O₃ in the *layered bottom layer* of the as-deposited films results in a *well-crystallized top layer* of maximum thickness. The increased surface homogeneity of the film that is observed upon the addition of the Ar annealing at 375 °C and 550 °C, can be explained by the phase transitions of the copper sulfide phases that occur in this temperature range in the absence of H₂S. At 375 °C, copper sulfide will presumably consist of β-Cu₂S, Cu₉S₅ and Cu_{1.81}S in accordance with the phases that were observed in the Spray ILGAR Cu_{2-x}S by XRD (Fig. 3.5¹⁷). In contrast, at 550 °C, β-Cu₂S is not stable anymore (Table 2.2.) and decomposes to copper and digenite Cu_{2-δ}S. Due to the fast diffusion of copper in digenite (section 4.3.), this excess-copper will interdiffuse between the digenite phases and may thus cause a more homogeneous distribution of copper sulfide on the surface.

¹⁶ Apart from CuInS₂, no phase was detected in the films after the H₂S and KCN treatments by XRD.

¹⁷ Since the diffractogram was obtained at room temperature, α-Cu₂S was observed instead of β-Cu₂S.

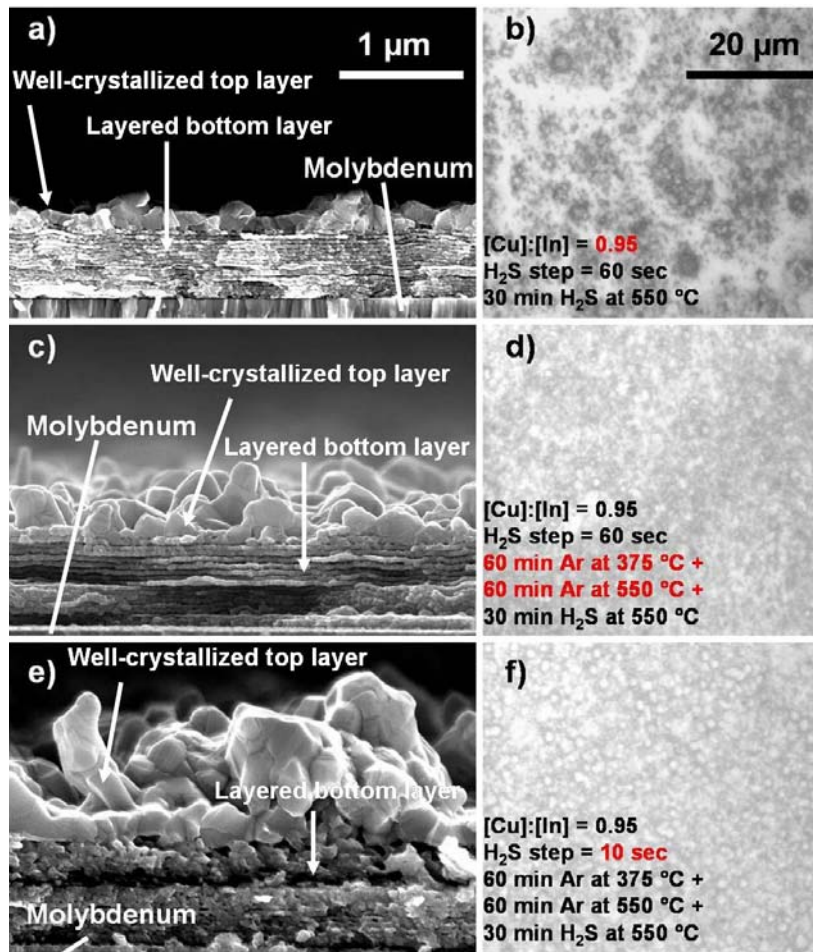


Fig. 4.18: Influence of preparation and annealing conditions on the morphology of the *well-crystallized top layer* of H₂S annealed Spray ILGAR CuInS₂ thin films:

Cross-sectional SEM and plan-view optical microscope images of H₂S annealed Spray ILGAR CuInS₂ thin films (samples 419 (a, b), 420 (c, d) and 421 (e, f). The varied preparation parameters are shown in Fig. b, d and f.

All other parameters were identical to those in Table 3.6.

In Appendix I, all preparation parameters are listed.

All SEM and optical micrographs are shown on the same scale, respectively.

See scale bar in a), b).

This will, consequently, result in a more homogeneous *well-crystallized top layer* as soon as copper sulfide is converted to CuInS₂ by the indiffusion of indium (as observed in Fig. 4.18b, d and e). This homogenization effect will not occur if H₂S is present during this annealing step, since all excess-copper would immediately react with H₂S and thus reduce the interdiffusion.

4.5. Growth Mechanism of Spray ILGAR CuInS₂ Thin Films

In this section, an overall model for the growth of the Spray ILGAR CuInS₂ thin films is summarized. The model is based on the processes described in sections 4.2. and 4.3. that explain the deposition and sulfurization of copper and In₂O₃ during the spray- and H₂S step of a single ILGAR-cycle. The subsequent diffusion processes (results of section 4.4.) that occur with the increased number of ILGAR-cycles are also considered (section 4.5.1.).

Subsequently, the diffusion processes during the post-deposition H₂S annealing are discussed in section 4.5.2. in order to explain the formation of the *well-crystallized top layer*.

4.5.1. Formation of As-Deposited Spray ILGAR CuInS₂ Thin Films

So far, the sulfurization of copper and In₂O₃, as well as the formation of CuInS₂ from In₂S₃ and Cu_{2-x}S have been discussed, as they are assumed to occur during a single spray step and the subsequent H₂S step of the ILGAR-cycle (section 4.3.; Fig. 4.11). From these considerations, the local distribution of Cu_{2-x}S, In₂O₃ and CuInS₂, which was observed in sections 4.4.2.1.-3., cannot be explained, yet. The effect of the carbon-rich interlayers on the growth process of the as-deposited Spray ILGAR CuInS₂ films also needs to be discussed.

If two or more ILGAR-cycles are applied in the Spray ILGAR process for CuInS₂ thin film deposition, in each cycle, copper (partially covered by hfac groups) and In₂O₃ are deposited in the spray step. In the following H₂S step, copper is completely converted to Cu_{2-x}S and In₂O₃ partially to In₂S₃. Subsequently, Cu_{2-x}S and In₂S₃ form CuInS₂ (Fig. 4.11). Thus, the material deposited in each ILGAR-cycle is present as a layer consisting of Cu_{2-x}S, In₂O₃ and CuInS₂. The layers grown by subsequent ILGAR-cycles are separated by carbon-rich interlayers, containing the residuals of the hfac groups (Fig. 4.17). However, due to the diffusion of copper out of the copper grains in the Cu_{2-x}S formation process (section 4.3.), the carbon-rich interlayers do not form a closed layer. The interdiffusion of copper, indium and sulfur between material deposited in subsequent cycles is unhindered along discrete diffusion paths. This is confirmed by the energy-filtered TEM images in Fig 4.17d, which show fluctuations in the interlayer thickness. A similar observation was made by Kaelin *et al.* for Cu(In,Ga)Se₂ thin films [Kaelin '05] deposited at 100 °C by doctor blading from a paste of copper and indium salts in a cellulose matrix. After annealing these films at 560 °C in selenium vapor, the authors observed a polycrystalline Cu(In,Ga)Se₂ layer located upon an amorphous carbon layer. Thus, it can be assumed that, although the interlayers prevent a continuous film growth in the Spray ILGAR process, they still allow diffusion of the elements to take place between the layers of material deposited in each ILGAR-cycle. In the following, diffusion processes are discussed, which can explain the distribution of Cu_{2-x}S, In₂O₃ and CuInS₂ that was observed in section 4.4.2.

Firstly, the segregation of Cu_{2-x}S agglomerates at the surface of the as-deposited Spray ILGAR CuInS₂ thin films is discussed. The segregation of binary copper phases on top of copper-rich prepared chalcopyrite thin films has been reported by various authors, independently of the deposition process that was applied [Klenk '93; Scheer '95; Rudigier '04; von Kloopmann '06]. This segregation can be explained by the fast diffusion of copper in copper sulfide phases as well as in CuInS₂ (section 4.3.). As it was shown in section 4.3., the diffusion length of copper in copper sulfide at 430 °C during a H₂S step of 20 s, can be calculated as $L_{D_{Cu_2S}^{Cu}} \approx 600 \mu\text{m}$ using the diffusion coefficients listed in Appendix V in Table V.1 and Eq. (4.11). For the diffusion of copper in CuInS₂, only the diffusion coefficient at 25 °C has been reported [Kleinfeld '88]. Since neither the frequency factor nor the activation energy was reported by these authors, the diffusion coefficient could not be calculated for a temperature of 430 °C. However, even at 25 °C, the lowest diffusion coefficient, which was reported by Kleinfeld *et al.* of $D_{CuInS_2}^{Cu} = 2.3 \cdot 10^{-9} \text{ cm}^2\text{s}^{-1}$ yields a diffusion length of $L_{D_{CuInS_2}^{Cu}} \approx 2.1 \mu\text{m}$ for a H₂S step duration of 20 s. Both values exceed the layer thickness of the investigated thin films (400-1000 nm) and thus show, that the Cu_{2-x}S segregation in the Spray ILGAR CuInS₂ deposition process can be explained by the diffusion of copper to the surface during the H₂S step of the ILGAR-cycle, no matter if the copper diffusion is assumed to proceed through Cu_{2-x}S or CuInS₂ domains. However, the fact that in the XAS and XPS measurements Cu_{2-x}S was observed on top of the CuInS₂ domains of the films, suggests that the diffusion proceeds through the CuInS₂ domains. That the segregation occurs at the surface of the films, is due to the fact that sulfur is provided from the surface in almost all deposition processes for chalcopyrite thin films (section 2.2). The chemisorption of sulfur atoms on the surface of chalcogenide (CuInS₂, Cu_{2-x}S, etc.) phases leads to the formation of a surface field, which accelerates the metal ions (cations) towards the surface [Pietzker '03]. That only the segregation of copper sulfide is observed, but no segregation of indium sulfide, is due to the fact that the diffusion of copper proceeds several orders of magnitudes faster than that of indium [Kleinfeld '88; Wissmann '97] (Table V.1; Fig. V.1).

It is also known that this segregation of copper sulfide causes a recrystallization of the chalcopyrite films, which increases the average grain size in the films [Neisser_2 '01; Klenk '93]. Neisser proposed a model for the Cu₂S-segregation in the growth of RTP-CuInS₂ thin

films¹⁸, according to which CuInS_2 that is present in the vicinity of a Cu_2S -region can partially (≤ 1 mol. %) dissolve in Cu_2S [Neisser_2 '01]. He assumed that the solubility of CuInS_2 in Cu_2S increases for increasing defect density. Once the maximum amount of CuInS_2 is dissolved, it will start to precipitate as CuInS_2 of reduced defect density. This results in a complete *migration* of CuInS_2 through the Cu_2S region. After this process, CuInS_2 of increased grain size and Cu_2S again exist as separate phases. This model was supported by Pietzker [Pietzker '03], who observed Cu_2S during the copper-rich growth of RTP- CuInS_2 by *in-situ* XRD.

This process may explain the three regions of different morphology, which were observed in the plan-view SEM image of the as-deposited and KCN etched Spray ILGAR CuInS_2 thin film in Fig. 4.15a (Fig. 3.12 and 4.15). The large agglomerates (about 1 μm) may consist of CuInS_2 grains, which were recrystallized by the segregation of Cu_{2-x}S . From there, the Cu_{2-x}S presumably extended over the surface, thereby covering the neighboring CuInS_2 grains, which were not recrystallized and therefore consist of smaller grains (some 100 nm). The rest of the layer may be assumed to consist of nanosized grains ($\ll 100$ nm) of In_2O_3 . As indicated by Raman measurements (section 5.2.2.), the In_2O_3 content decreases in depth, which is presumably due to the nanocrystalline morphology of the films, which allows H_2S to penetrate into the film during the H_2S step, so that it can reach In_2O_3 that was deposited in previous ILGAR-cycles. Hence, the In_2O_3 in the lower part of the films is exposed to more H_2S steps than the In_2O_3 in the upper part. Consequently, the lower part will contain less In_2O_3 .

Fig. 4.19 schematically depicts the composition of the as-deposited Spray ILGAR CuInS_2 thin films and the paths of Cu_{2-x}S segregation according to the growth model, which has been proposed in this section. The *layered bottom layer* consists of nanocrystalline CuInS_2 - and In_2O_3 -containing layers of 30 nm thickness, which are separated by carbon rich interlayers. On top of the film, Cu_{2-x}S agglomerates are found, which were formed by the fast diffusion of copper through the CuInS_2 domains of the film.

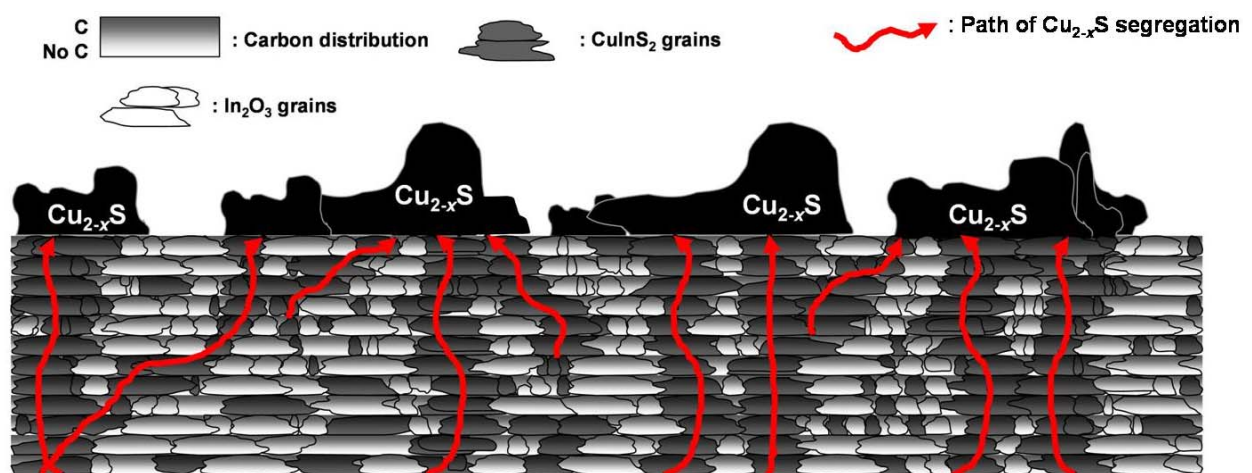


Fig. 4.19: Schematic sketch of the composition of the as-deposited Spray ILGAR CuInS_2 thin films according to the growth model proposed in this section. Additionally, the paths of Cu_{2-x}S segregation are indicated.

4.5.2. Diffusion Processes during the Post-Deposition H_2S annealing

This section focuses on the diffusion processes during the post-deposition H_2S annealing of as-deposited Spray ILGAR CuInS_2 thin films, which leads to the formation of the *well-crystallized top layer* on top of the *layered bottom layer* (Fig. 3.13). In particular, the sulfurization of the residual In_2O_3 in the as-deposited films and the subsequent CuInS_2 -

¹⁸ Cu_2S is converted to CuS in this process during the cooling of the film in a sulfur-containing atmosphere. It was shown, however, that it originally segregates as Cu_2S and is converted subsequently [Pietzker '03].

formation is discussed.

It was found that after a post-deposition H₂S annealing and a subsequent KCN etching - besides the carbon-rich interlayers - the Spray ILGAR CuInS₂ thin films completely consist of CuInS₂ (section 4.4.1.). The KCN etching leads to the removal of all segregated Cu_{2-x}S that is accessible from the film surface. The KCN etching of CuInS₂ films is well-investigated [Scheer '94; Scheer '95; Weber '02] and therefore not discussed in the following.

In contrast to the sulfurization process during the H₂S step of the ILGAR-cycle (section 4.3.), the post-deposition H₂S annealing leads to a complete sulfurization of the In₂O₃ in the as-deposited Spray ILGAR CuInS₂ thin films (Fig. 4.12). Why this is the case, is discussed in the following. The post-deposition annealing is performed at a temperature of 550 °C. Although this temperature is higher than the deposition temperature of 430 °C, it only leads to a small increase (<3 %) of the free energy ($\Delta G_{427\text{ °C}} = -101286\text{ J mol}^{-1}$ and $\Delta G_{627\text{ °C}} = -104415\text{ J mol}^{-1}$ for Eq. (4.2); Appendix X., [Knacke '91]). Thus, it is unlikely that the completion of the sulfurization of In₂O₃ in the post-deposition annealing is just a result of a higher temperature.

As shown in sections 4.4.2.1 and 4.4.2.2., In₂O₃ and CuInS₂ are located in the *layered bottom layer* of the as-deposited Spray ILGAR CuInS₂ thin films, whereas Cu_{2-x}S segregates on top of the CuInS₂ domains of the films (Fig. 4.14-15, 4.19). Furthermore, it was shown that the *well-crystallized top layer* that is formed during the post-deposition H₂S annealing consists of CuInS₂ (Fig. 4.16).

From the three species copper, indium and sulfur, copper diffuses the fastest at any given temperature in CuInS₂ (Appendix V; Table V.1; Fig. V.1: $D^{\text{Cu}}_{\text{CuInS}_2} = 2.3 \cdot 10^{-9} - 3.2 \cdot 10^{-6}\text{ cm}^2\text{s}^{-1}$ at 25 °C [Kleinfeld '88]; $D^{\text{In}}_{\text{CuInS}_2} = 2.7 \cdot 10^{-10} - 1.9 \cdot 10^{-8}\text{ cm}^2\text{s}^{-1}$ at 650 °C [Wissmann '97]; and $D^{\text{S}}_{\text{CuInS}_2} = 1 \cdot 10^{-16}\text{ cm}^2\text{s}^{-1}$ at 575 °C; [Titus '06]). Hence, it would be expected that for a stack of Cu_{2-x}S/CuInS₂/In₂S₃, the diffusion of copper from Cu_{2-x}S through CuInS₂ into In₂S₃ is the dominant process, rather than the diffusion of indium in the opposite direction. It will be explained in the following that the opposite seems to be the case in the Spray ILGAR CuInS₂ process.

During the formation of the *top layer*, the number of the thin layers in the *layered bottom layer* does not change. This indicates that the *well-crystallized top layer* is formed by the diffusion of indium out of the In₂O₃-domains in the *layered bottom layer* into the Cu_{2-x}S agglomerates on the film surface upon H₂S annealing. If the *well-crystallized top layer* was formed by the diffusion of copper into the In₂S₃ domains that are formed by the sulfurization of In₂O₃, the *well-crystallized top layer* should be formed at the expense of the *layered bottom layer*. This should thus lead to a reduction of the number of layers in the *layered bottom layer*, which is not observed (Fig. 3.13c, d).

However, all experimental observations of the previous sections can be explained, if one regards the accessibility of H₂S to the sulfurization reaction sites as the reaction-limiting factor. This also agrees with the previous conclusion that the incomplete sulfurization of In₂O₃ in the Spray ILGAR processes of In₂(O,S)₃, as well as of CuInS₂ thin films (section 4.3.), was proposed to be limited by the slow diffusion of oxygen through the In₂S₃ layer, which is formed on top of the In₂O₃ domains of the film after the sulfurization of the upmost In₂O₃ monolayers (Fig. 4.11).

Due to the slow oxygen-diffusion in In₂S₃, the sulfurization of In₂O₃ to In₂S₃ by H₂S (Eq. (4.17-19)), which is a prerequisite to the formation of CuInS₂, can be assumed to be the rate-limiting reaction. H₂S needs to access the reaction site and H₂O, as a product, needs to be able to leave it (Section 4.3.). Taking this into account, the processes occurring during the post-deposition H₂S annealing of the as-deposited Spray ILGAR CuInS₂ thin films, can be understood as a continuous sequence of the sulfurization of surface In₂O₃ and the subsequent diffusion of indium into the Cu_{2-x}S agglomerates on top of the film. This mechanism is visualized in Fig. 4.20a-d and is explained in the following. Since, according to the presented model, the sulfurization of In₂O₃ to In₂S₃ by H₂S proceeds mainly at the surface of the In₂O₃

grains, only a small volume of the interface between the top of the *layered bottom layer* of the film and the Cu_{2-x}S agglomerates on the film surface is depicted in Fig. 4.20. The green arrows indicate that H_2S approaches the film from the surface.

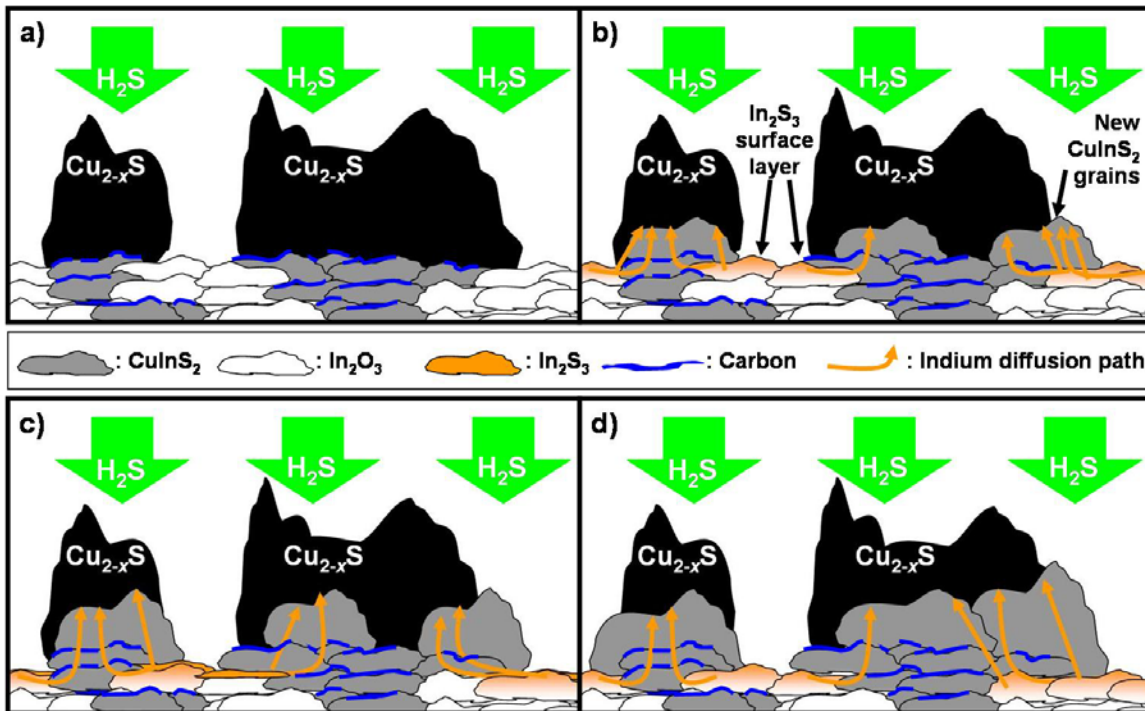


Fig. 4.20: Schematic sketch of the diffusion processes that are proposed to occur during the post-deposition H_2S annealing of the as-deposited Spray ILGAR CuInS_2 thin films. a) State of the as-deposited Spray ILGAR CuInS_2 thin film prior to a reaction with H_2S . b) The upmost surface of the In_2O_3 regions of the as-deposited Spray ILGAR CuInS_2 thin film is sulfurized to In_2S_3 by H_2S . Cu_{2-x}S and In_2S_3 start to react to CuInS_2 , where they are in contact to each other. Additionally, CuInS_2 can be formed by indium diffusion through CuInS_2 grains into the Cu_{2-x}S agglomerates. b) Further consumption of the upmost In_2O_3 domains and further formation of CuInS_2 on top of the *layered bottom layer*. c-d) After all In_2O_3 of the upmost layer of the *layered bottom layer* is consumed, the In_2O_3 grains in the next layer become accessible to H_2S and can be sulfurized subsequently. Thus, all In_2O_3 in the film can be completely consumed without any kinetic hindrance. Thereby the *well-crystallized top layer* is formed by the new CuInS_2 grains (indicated in (b)).

At the very beginning of the post-growth H_2S annealing, only the In_2O_3 at the surface of the film, which is not covered by Cu_{2-x}S , is accessible to H_2S (Fig. 4.20a). Additionally, some deeper In_2O_3 might also be accessible due to voids or cracks in some areas of the film. These In_2O_3 domains will be firstly converted to In_2S_3 (Fig. 4.20b). As soon as In_2S_3 is formed, interdiffusion processes of indium, copper and sulfur can start, wherever Cu_{2-x}S or CuInS_2 are in contact with In_2S_3 . In principle, all three elements can diffuse in all directions, which may indeed be the case in the very first moments of the process. However, copper that diffuses into In_2S_3 will cause the coverage of the In_2O_3 grain with CuInS_2 . This will prevent any further contact between the covered residual In_2O_3 and H_2S as soon as all In_2S_3 has been converted to CuInS_2 . Thus the reaction rate will decrease as soon as all open In_2O_3 surface is covered. Then the reaction can only proceed if oxygen diffuses through the CuInS_2 shell. This can be assumed to be a much slower process, since the diffusion rate of anions in CuInS_2 is about 5-6 orders of magnitudes smaller than the cation diffusion rate. Furthermore, the diffusion of copper into the $\text{In}_2\text{S}_3/\text{In}_2\text{O}_3$ grain is unlikely, since the presence of H_2S at the surface promotes the diffusion of copper towards the film surface and thus hinders its diffusion from the surface agglomerates into the *layered bottom layer* (section 4.5.1.).

In contrast, the diffusion of indium out of the In_2S_3 surface layer into Cu_{2-x}S grains (either

directly or through CuInS₂ grains) will lead to the consumption of In₂S₃ and thus to the sulfurization of further In₂O₃ (Fig. 4.20b-c). Therefore, this diffusion process can continue without any decrease of the reaction rate until all In₂O₃ is completely consumed, since there will be always open In₂O₃ surfaces accessible to H₂S. After the complete conversion and consumption of the In₂O₃ grain a nanosized void remains where the grain used to be (Fig. 4.20d). This allows the H₂S to get in contact with the In₂O₃ grains of the next layer of the *layered bottom layer*, where the same procedure can take place again.

Thus, according to the proposed model, the In₂O₃ grains of every single layer in the *layered bottom layer* of are sequentially sulfurized during the post-deposition H₂S annealing, which then enables the diffusion of indium away from the grain and thus from the reaction site either directly into Cu_{2-x}S or through a neighboring CuInS₂ grain. Finally, the diffusing indium will reach the Cu_{2-x}S agglomerates on top of the films, where it will lead to the precipitation of CuInS₂. Since on top of the film H₂S is present in excess and indium enters the agglomerates from below, the reaction is neither kinetically nor diffusion-limited and can proceed freely. This then leads to the growth of the large CuInS₂ crystallites that form the *well-crystallized top layer* in the H₂S annealed Spray ILGAR CuInS₂ films. Depending on the [Cu]:[In] ratio of the spraying solution, Cu_{2-x}S will either be completely consumed or some of it may remain on the surface. In this case it has to be removed by a subsequent KCN etching.

In conclusion, the model for the diffusion processes that occur during the post-deposition H₂S annealing of the as-deposited Spray ILGAR CuInS₂ thin films can be subdivided into the following subprocesses, which occur successively in each layer of the *layered bottom layer* of the films until all In₂O₃ has been sulfurized and the *well-crystallized top layer* has been formed on the film surface:

- Sulfurization of surface In₂O₃ to In₂S₃
- Lateral indium diffusion through the In₂S₃ surface layer towards either an In₂S₃/Cu_{2-x}S or an In₂S₃/CuInS₂ interface
- Diffusion of indium through CuInS₂ towards an CuInS₂/Cu_{2-x}S interface
- Formation of CuInS₂ from In₂S₃ and Cu_{2-x}S

Finally, the proposed model should be tested quantitatively. Therefore, each of these subprocesses is considered separately, based on reported diffusion coefficients for copper, indium and sulfur, which are summarized in Appendix V in Table V.1 and Fig. V.1.

It has been shown that a H₂S annealing of 15 min at 550 °C was sufficient to sulfurize all In₂O₃ in an as-deposited Spray ILGAR CuInS₂ thin film of a thickness of about 1 μm (Tables 4.2-4; sample 329). According to the proposed model, an indium atom must thus be able to diffuse over a length of up to 1 μm from an In₂O₃ grain at the molybdenum layer to the Cu_{2-x}S agglomerates on the film surface.

Indium Diffusion through Cu_{2-x}S and CuInS₂

Assuming, that the diffusion coefficients of $D_{\text{Cu}_2\text{Se}}^{\text{In}} = 4.2 \cdot 10^{-6} \text{ cm}^2\text{s}^{-1}$ for the diffusion of indium in Cu₂Se at 650 °C [Park '00] and of $D_{\text{CuInS}_2}^{\text{In}} = 2.7 \cdot 10^{-10} \text{ cm}^2\text{s}^{-1}$ [Wissmann '00] for the diffusion of indium in CuInS₂ at 650 °C, are also valid for the diffusion of indium in Cu₂S and CuInS₂ at 550 °C, the diffusion lengths for the diffusion of indium are calculated according to Eq. (4.11) as $L_{D_{\text{Cu}_2\text{S}}^{\text{In}}} = \sqrt{D_{\text{Cu}_2\text{S}}^{\text{In}} \cdot 900 \text{ sec}} \approx 610 \text{ μm}$ in Cu₂S and $L_{D_{\text{CuInS}_2}^{\text{In}}} = \sqrt{D_{\text{CuInS}_2}^{\text{In}} \cdot 900 \text{ sec}} \approx 5 \text{ μm}$ in CuInS₂ within a duration of 15 min. Both values exceed the thickness of the film. Thus, the diffusion of indium through the entire film within a duration of 15 min seems possible even at a lower temperature of 550 °C. In particular, it can be assumed that the diffusion coefficients are even larger in the Spray ILGAR process due to the porous and nanocrystalline structure of the *layered bottom layer* of the films, which provides additional diffusion paths (section 4.1.).

Lateral Diffusion of Indium in In_2S_3

The diffusion of indium in In_2S_3 or in the closely related In_2Se_3 has not been investigated to date to the knowledge of the author. However, the diffusion of sulfur in In_2S_3 has been studied by Tezlevan *et al.* [Tezlevan '93], whereas the diffusion of indium in the interface region of an $\text{In}_2\text{Se}_3/\text{CuGaSe}_2$ diffusion couple was analyzed by Djessas *et al.* [Djessas '04]. From these reports some conclusions about the diffusion of indium in In_2S_3 can be drawn. Tezlevan *et al.* determined the frequency factor and activation energy for the diffusion of sulfur in sc- In_2S_3 as $134.23 \text{ cm}^2\text{s}^{-1}$ and 1.51 eV, respectively [Tezlevan '93]. Using Eq. (4.11), this yields a diffusion length of $L_{D_{\text{In}_2\text{S}_3}^{\text{S}}} \approx 80 \text{ }\mu\text{m}$ for a duration of 15 min at a temperature of 550 °C. Since, in the spinel In_2S_3 lattice, 1/9 of the indium sites are empty, whilst all sulfur sites are occupied, the diffusion length for the diffusion of indium in In_2S_3 , is likely to exceed this value. Djessas *et al.* reported a frequency factor and activation energy of $8 \cdot 10^{-11} \text{ cm}^2\text{s}^{-1}$ and 0.32 eV, respectively for the diffusion of indium in an $\text{In}_2\text{Se}_3/\text{CuGaSe}_2$ diffusion couple [Djessas '04]. For a duration of 15 min at a temperature of 550 °C, this results in a diffusion length of $L_{D_{\text{In}_2\text{Se}_3/\text{CuGaSe}_2}^{\text{In}}} \approx 280 \text{ nm}$. The indium diffusion in an $\text{In}_2\text{Se}_3/\text{CuGaSe}_2$ diffusion couple is likely to be limited by the slow diffusion of indium in the chalcopyrite lattice of CuGaSe_2 , rather than by the indium diffusion in In_2Se_3 (Table V.1; [Djessas '04]), so that the diffusion length of indium in In_2S_3 is likely to exceed 280 nm during the post-deposition H_2S annealing. Based on these published data of Tezlevan *et al.* and Djessas *et al.*, it can be concluded that the diffusion length of indium is at least of the order of several hundred nm, even though a diffusion length of about 100 μm is more likely. In Fig. 4.15, it was observed that the In_2O_3 -containing regions have diameters of the order of 5-10 μm and consist of grains with an average size below 100 nm. Hence, based on the above consideration about the diffusion length of indium in In_2S_3 it seems likely that indium can diffuse through the In_2S_3 surface layer on top of the In_2O_3 grains and reach the $\text{In}_2\text{S}_3/\text{Cu}_{2-x}\text{S}$ or $\text{In}_2\text{S}_3/\text{CuInS}_2$ interfaces in order to form CuInS_2 .

Sulfurization of In_2O_3 by Oxygen Diffusion through an In_2S_3 Surface Layer

Based on the assumptions about the diffusion of oxygen through the In_2S_3 surface layer, which forms on the In_2O_3 grains upon H_2S annealing (section 4.3.), the diffusion coefficient for this process was estimated by a frequency factor $D_0^{\text{O}}_{\text{In}_2\text{S}_3} \approx D_0^{\text{S}}_{\text{In}_2\text{S}_3} = 134.2 \text{ cm}^2\text{s}^{-1}$ and an activation energy $2.0 \text{ eV} \leq E_A^{\text{O}}_{\text{In}_2\text{S}_3} \leq 2.4 \text{ eV}$. If the diffusion length for oxygen diffusing through In_2S_3 is calculated from Eq. (4.11) based on these assumption, this yields $155 \text{ nm} \leq L_{D_{\text{In}_2\text{S}_3}^{\text{O}}} \leq 2.6 \text{ }\mu\text{m}$ for an annealing duration of 15 min and a temperature of 550 °C. The actual thickness of 1 μm of the as-deposited Spray ILGAR thin film that was completely sulfurized within 15 min of post-deposition annealing (sample 329) lies in between these values. Thus, the complete conversion of all In_2O_3 in the film could possibly be explained by the diffusion of oxygen through the surface In_2S_3 layer without any lateral diffusion of indium in In_2S_3 , which leads to the exposure of further In_2O_3 and thus enhances the sulfurization rate. In order to verify this, a sprayed pc- In_2O_3 thin film of $630 \pm 95 \text{ nm}$ (ERDA) thickness was prepared analogously to the In_2O_3 thin film (sample 402), which was described in section 4.2.2. and annealed in H_2S for 45 min at 550 °C. After this H_2S annealing, the X-ray diffractogram of this film proved that the film still contained In_2O_3 as a secondary phase and was thus not completely sulfurized. This shows that for a H_2S annealing of 45 min at 550 °C, the diffusion length of oxygen is below $630 \pm 95 \text{ nm}$ corresponding to a diffusion coefficient of $D^{\text{O}}_{\text{In}_2\text{S}_3} \leq (1.5 \pm 0.5) \cdot 10^{-12} \text{ cm}^2\text{s}^{-1}$. Consequently, it can be concluded that the sulfurization of In_2O_3 during the post-deposition H_2S annealing of the as-deposited Spray ILGAR CuInS_2 thin films, cannot be solely explained

by the diffusion of oxygen through In_2S_3 , but has to be assisted by the lateral transport of indium in this In_2S_3 layer towards $\text{In}_2\text{S}_3/\text{Cu}_{2-x}\text{S}$ or $\text{In}_2\text{S}_3/\text{CuInS}_2$ interfaces, which provides newly accessible In_2O_3 surfaces and thus further enhances the sulfurization rate.

In conclusion, these quantitative considerations show that the model for the H_2S annealing process can explain the complete sulfurization of In_2O_3 and the formation of the *well-crystallized top layer* qualitatively as well as quantitatively.

In summary, the models for the growth of the as-deposited and of the H_2S annealed Spray ILGAR CuInS_2 thin films, which were proposed in sections 4.5.1 and 4.5.2., respectively, are able to explain all the experimental observations presented in section 4.2.-4.. In particular, these models can explain the peculiar and initially puzzling bilayered morphology of the H_2S and KCN treated Spray ILGAR CuInS_2 thin films (section 3.3.2; Fig. 3.13).

4.6. Consequences of the Growth Model for the Spray ILGAR Process

In the following, the addition of H_2O to the spraying solution in the Spray ILGAR deposition process for CuInS_2 thin films as a future process modification is suggested. This suggestion is based on the growth model, which was deduced for these films in sections 4.2.-5. Preliminary results obtained using such a modified process are also briefly discussed.

It was shown in section 4.2.3 that the addition of H_2O to the spraying solution in the Spray ILGAR CuInS_2 deposition process leads to an increased copper-incorporation into the film (Table 4.1). On the basis of the copper deposition mechanism proposed in section 4.2.1., this was explained by the removal of adsorbed hfac groups from the deposited copper by H_2O , which prevents the blocking of copper deposition sites by these groups (Fig. 4.3). These adsorbed hfac groups have been identified as the origin of the carbon-containing interlayers, which are observed in the *layered bottom layer* of the Spray ILGAR CuInS_2 thin films (Fig. 3.13). Therefore, it is predicted that the addition of H_2O to the spraying solutions, should prevent the formation of these carbon-containing interlayers. This prediction was tested in a preliminary deposition experiment, in which a Spray ILGAR CuInS_2 thin film was deposited from a spraying solution consisting of 15 ml of 40 mM $\text{Cu}(\text{hfac})_2/\text{acetone}$, 10 ml of 40 mM $\text{InCl}_3/\text{acetone}$ and 2 ml of Millipore™ H_2O using standard deposition parameters as they have been deduced in section 3.3.2. (Appendix I). After deposition, the film was annealed in $\text{Ar}/\text{H}_2\text{S}$ at 550 °C (Appendix I) and characterized by SEM and XRD afterwards (Fig. 4.21):

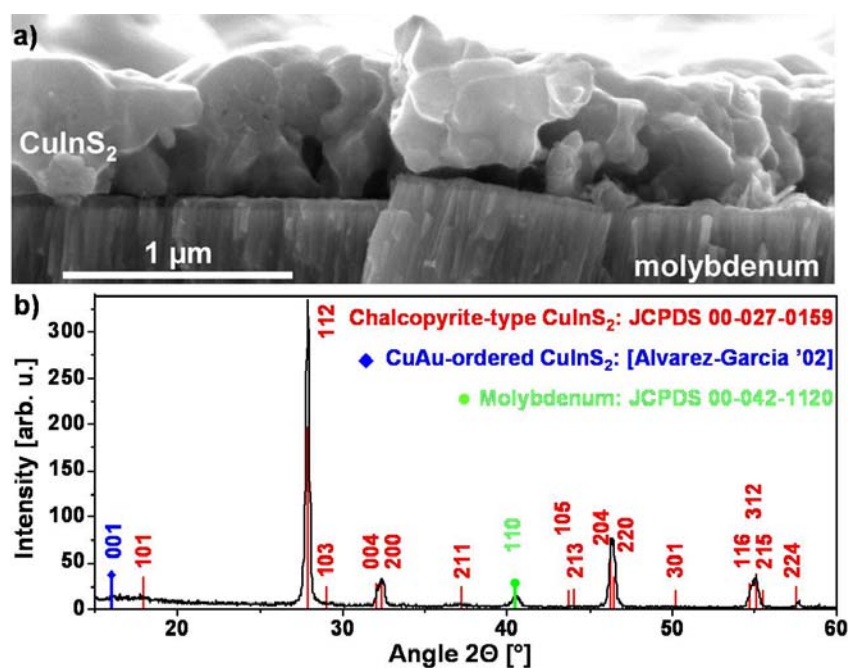


Fig. 4.21: a) Cross-sectional SEM image of a H_2S annealed Spray ILGAR CuInS_2 thin film (sample 422), which was prepared from a H_2O -containing spraying solution. b) X-ray diffractogram of the same film. The diffractogram was recorded in grazing incidence mode (0.5°). A list with the detailed preparation parameters can be found in Appendix I.

The characterization of such deposited Spray ILGAR CuInS₂ thin film revealed that the film did not exhibit a layered morphology and thus confirmed the prediction deduced from the growth model. In Fig. 4.21a, a cross-sectional SEM image of this Spray ILGAR CuInS₂ thin film is shown. As predicted by the model, the film shows a compact morphology. XRD measurements, confirmed that the deposited film consisted of CuInS₂ (Fig. 4.21b).

This preliminary result shows that the layered morphology of the Spray ILGAR CuInS₂ thin films can be overcome by the addition of H₂O to the spraying solution, which supports the validity of the proposed growth model. However, no optimization of the Spray ILGAR CuInS₂ deposition process based on H₂O-containing spraying solutions has been performed, yet. Furthermore, so far neither the structural nor the photovoltaic properties of the layered Spray ILGAR CuInS₂ thin films have been analyzed in detail. Therefore, the remainder of this thesis focuses on the analysis of the properties of the Spray ILGAR CuInS₂ thin films, which are prepared without the addition of H₂O using the process described in section 3.3.2. Nevertheless, the addition of H₂O remains a promising process modification for the future.

4.7. Summary of Chapter 4

In this chapter, each stage (spray step, H₂S step, post-deposition H₂S annealing) involved in the growth of Spray ILGAR CuInS₂ thin films, has been analyzed separately by identifying the compounds and distribution in the resulting layers or films. Based on this analysis a growth model was proposed that can explain all experimental observations, including the bilayered morphology of the Spray ILGAR CuInS₂ thin films (Fig. 3.13).

In section 4.2., it was shown that copper and In₂O₃ are deposited as copper- and indium-containing precursor compounds during the spray step of the Spray ILGAR deposition process of CuInS₂. This was achieved by firstly analyzing both deposition processes separately. Based on this analysis, deposition mechanisms for both compounds could be proposed. The mechanisms revealed that the deposition processes of In₂O₃ and copper both depend on the availability of H₂O during the growth process. In the copper deposition from Cu(hfac)₂ solutions, H₂O serves as a catalyst for the removal of hfac groups from the deposited copper, whereas it is consumed in the hydrolysis of InCl₃ in the In₂O₃ deposition process. In the Spray ILGAR deposition process for CuInS₂ both processes occur simultaneously with only small amounts of H₂O present in the spraying solution. Due to this limited amount of H₂O, both deposition processes interfere with each other, such that the hfac groups cannot be removed from the deposited copper. This leads to the (partial) coverage of the deposited precursor layer with adsorbed hfac groups, which results in the dependence of the [Cu]:[In] ratio on the spray step duration. It was shown that the addition of H₂O to the spraying solution leads to an enhanced copper deposition rate and thus to an increase of the [Cu]:[In] ratio of the deposited layer.

The sulfurization of the precursor layer, which was deposited in the spray step, during the H₂S step of the ILGAR-cycle, was discussed in section 4.3. By considering the different diffusion processes during the sulfurization of copper and In₂O₃, it could be explained, why copper was completely converted to Cu_{2-x}S (0 ≤ x ≤ 0.2), whilst the sulfurization of In₂O₃ was incomplete. It was revealed that the sulfurization of copper by H₂S can proceed within the H₂S step duration by the diffusion of copper out of the copper grain to its surface. In contrast, the sulfurization of In₂O₃ was limited by the diffusion of oxygen through the In₂S₃ surface layer that forms on top of the In₂O₃ domains, so that only a surface-near region of the latter could be converted to In₂S₃ in each ILGAR-cycle.

In section 4.4., the composition and morphology of the as-deposited, as well as of the H₂S and KCN treated Spray ILGAR CuInS₂ thin films was studied. It was shown that depending on the preparation conditions, the as-deposited films contain up to 32 ± 6 mol. % Cu_{2-x}S, 25 ± 2 mol. % In₂O₃ and about 5 ± 1 at. % of carbon as secondary phases. By combining

various analysis techniques (SEM, XRF, ERDA, XPS, XAS, TEM and EDX), it could be revealed that In_2O_3 and CuInS_2 coexist in form of 30 nm thin layers in the *layered bottom layer* of the as-deposited films. These layers are separated by interlayers of a yet unknown carbon-containing compound. Cu_{2-x}S was found in form of agglomerates on top of the CuInS_2 domains of the as-deposited films. Furthermore, the morphology of the *well-crystallized top layer*, which was formed during the post-deposition H_2S annealing, was found to depend on the In_2O_3 content of the as-deposited film (thickness), as well as on the annealing duration (homogeneity).

Based on the results of section 4.4., growth models for the deposition of the as-deposited Spray ILGAR CuInS_2 thin films, as well as for the formation of the *well-crystallized top layer*, could be proposed in section 4.5. According to these models the growth of the Spray ILGAR CuInS_2 thin films is governed by two dominant diffusion processes. During the growth of the as-deposited films, the main diffusion process is the segregation of Cu_{2-x}S on top of the CuInS_2 domains. This process could be described by a model proposed by Neisser for the growth of RTP- CuInS_2 thin films [Neisser_2 '01]. In contrast, the dominant diffusion process during the post-deposition H_2S annealing is the diffusion of indium into the Cu_{2-x}S agglomerates, where it leads to the formation of the *well-crystallized top layer*. In both processes, the formation rate of CuInS_2 is limited by the sulfurization rate of In_2O_3 , which was concluded to depend on the accessibility of the In_2O_3 surface for H_2S . As soon as the In_2O_3 grain is covered by a surface layer of In_2S_3 , the sulfurization of the underlying In_2O_3 can only proceed by the diffusion of oxygen through this layer, which was estimated to be a slow diffusion process ($D_{\text{In}_2\text{S}_3}^{\text{O}} \leq (1.5 \pm 0.5) \cdot 10^{-12} \text{ cm}^2\text{s}^{-1}$ at 550 °C). The activation energy of this diffusion process was estimated to lie between 2.0 eV and 2.4 eV.

In conclusion, the analysis of the Spray ILGAR CuInS_2 growth process in this chapter explains the formation process of the films and thus provides a valuable basis for process modifications in order to further improve the properties of the films with respect to their photovoltaic properties. In particular, it was shown that the addition of water to the spraying solution is a promising way to avoid the carbon-contamination of the films and thus also their layered morphology.

In order to verify the models, which were proposed for the growth of Spray ILGAR CuInS_2 thin films, *in-situ* experiments that monitor the growth of the films in real-time, would be highly desirable for the future. Similar experiments have been performed by Rudigier and Pietzker for the growth of RTP- CuInS_2 thin films using Raman Spectroscopy and XRD, respectively [Rudigier_01 '04; Pietzker '03]. In the case of the Spray ILGAR process, also *in-situ* mass spectroscopy or thermogravimetry appear to be promising for monitoring the deposition of the precursor compounds during the spray step of the ILGAR-cycle.